Spring 2007

Direct simulations of cells motions and deformations in flow

Quan Jin
New Jersey Institute of Technology

ABSTRACT

DIRECT SIMULATIONS OF CELLS MOTIONS AND DEFORMATIONS IN FLOW

by
Quan Jin

Direct numerical simulations (DNS) are used to study the motions and deformations of blood cells, especially leukocytes, in pressure driven flows in parallel plate channels with both smooth and uneven walls under adhesion force between the leukocytes and the channel wall.

Leukocytes are represented by two composite fluid models. The first model is the compound-drop model in which the cytoplasm and the nucleus are modeled as fluids, and the second one is the drop-rigid-particle model in which the cytoplasm is modeled as a fluid and the nucleus as a rigid particle. The adhesion force is computed using two adhesion force models. In the first model, the adhesion force is given by a potential, and in the second model it is given by Dembo's kinetic adhesion model. The numerical code is based on the finite element method and the level-set technique is used to track the cell membrane position.

In the absence of the adhesion force, in a pressure driven flow the leukocyte moves away from the wall to an equilibrium location. In presence of the adhesion force, provided it is located within the range of the force, the leukocyte is attracted to the layer of endothelial cells and it flattens under the action of hydrodynamic forces. It is found that for the normal parameter values and flow rates the adhesive force given by the kinetic model is too small to capture the leukocyte. The time at which all bonds are broken and the leukocyte moves away from the wall increases when the capillary

number is increased, and decreases with increasing Reynolds number. The former suggests that the adhesion tendency of a leukocyte increases as its cortical tension is reduced. The distance traveled by a leukocyte before all bonds are broken increases with the Reynolds and capillary numbers. The rolling velocity of the leukocyte near an uneven wall varies in the sense that it appears to slip when its lower surface is in the gap between the spheres and stick when it comes close to the spheres' surfaces, which is in qualitative agreement with the experimental data.

DIRECT SIMULATIONS OF CELLS MOTIONS AND DEFORMATIONS IN FLOW

by
Quan Jin

A Dissertation
Submitted to the Faculty of
New Jersey Institute of Technology
in Partial Fulfillment of the Requirements for the Degree of
Doctor of Philosophy in Mechanical Engineering

Department of Mechanical Engineering

May 2007

APPROVAL PAGE

DIRECT SIMULATIONS OF CELLS MOTIONS AND DEFORMATIONS IN FLOW

Quan Jin

Dr. Pushpendra Singh, Dissertation Advisor Professor of Mechanical Engineering, NJIT	Date
Dr. Ian S. Fischer, Committee Member Professor of Mechanical Engineering, NJIT	Date
Dr. I. Joga Rao, Committee Member Associate Professor of Mechanical Engineering, NJIT	Date
Dr. Rong-yaw Chen, Committee Member Professor of Mechanical Engineering, NJIT	Date
Dr. Dentcho V. Ivanov, Committee Member Research Professor, Biomedical Engineering, NJIT	Date

BIOGRAPHICAL SKETCH

Author: Quan Jin

Degree: Doctor of Philosophy

Date: May 2007

Undergraduate and Graduate Education:

- Doctor of Philosophy in Mechanical Engineering,
  New Jersey Institute of Technology, Newark, NJ, 2007

- Master of Science in Thermal Engineering,
  Tsinghua University, Beijing, P. R. China, 2000

- Bachelor of Science in Civil Engineering,
  Qingdao Institute of Architecture and Engineering, Shandong, P. R. China, 1997

Major: Mechanical Engineering

Presentations and Publications:

Q. Jin, C. Verdier, P. Singh and N. Aubry

"Migration and deformation of leukocytes in pressure driven flow", *Journal of Fluid Engineering ASME*, submitted 2007.

Q. Jin, C. Verdier, P. Singh, N. Aubry, A. Duperray.
"Migration, rolling and deformation of circulating cells adhering to a wall under flow", FEDSM2006-98415 Symposium Paper, *ASME* 2006.

Q. Jin, C. Verdier, P. Singh, N. Aubry, A. Duperray.
"Direct simulation of the migration of leukocytes in pressure driven flow", *ASME 2nd Joint U.S.-European Fluids Engineering Summer Meeting*, Miami, FL, 2006.

Q. Jin, Verdier, C., Singh, P.
"Rolling and deformation of cells in pressure driven flows", *the 56th Annual Meeting of the Division of Fluid Dynamics, American Physical Society*, New Jersey, November 2003.

C. Verdier, Q. Jin, P. Singh, et al,
"Modeling the rolling and deformation of a circulating cell adhering on an adhesive wall under flow", *Archives of Physiology and Biochemistry*, **111** Spp l., 14, 2003

To my beloved family

ACKNOWLEDGMENT

During these years in New Jersey Institute of Technology, the author's research advisor, Professor Pushpendra Singh, provided invaluable guidance and encouragement in her study and research. The author would like to express her great appreciation to Dr. Singh's advising and consider her to be very lucky to be under the guidance of such a remarkable scientist.

The author would like to thank Professors I. Joga. Rao, Rong-yaw Chen, Ian S. ischer and Dentcho V. Ivanov who provided suggestions as members of the committee.

The author also wants to thank the Graduate Studies office staff, Mrs. Gonzáles, Dr. Kane, Mr Grundy for their help during the study time.

In the end, the author would like to thank her family for their support and encouragement all the time.

TABLE OF CONTENTS

Chapter	Page
1 INTRODUCTION	1
1.1 Objective	1
1.2 Background	3
2 REVIEW OF PREVIOUS STUDIES ON DROPS DYNAMICS IN FLOWS	7
2.1 Free-Boundary Problems	7
2.2 Studies of Drops and Cells Deformation	7
2.2.1 Small Deformation Theories	8
2.2.2 Experimental Studies of Drops and Cells Deformation	11
2.2.3 Numerical Approaches	14
2.3 Lateral Migration of Drops and Particles	20
2.3.1 Experimental Studies	21
2.3.2 Analytical Studies	21
2.3.3 Numerical Work	22
3 RHEOLOGICAL MODELS OF LEUKOCYTE	24
3.1 Drop – Rigid Particle Model	27
3.2 Composite Drop Model	27
4 ADHESION MODELS	30
4.1 Adhesion Potential	30
4.2 Kinetic Adhesion Model	31
4.2.1 Rate Constants of Bonds Formation	32

TABLE OF CONTENTS
(Continued)

Chapter	Page
4.2.2 Analysis of the Kinetic Model for Bonds Formation	34
5 GOVERNING EQUATIONS	42
5.1 Problem Description	42
5.2 Governing Equations	43
5.3 Nondimensionlization of the Governing Equations	46
6 NUMERICAL APPROACH	48
6.1 Level Set Method	49
6.2 Reinitialization of ϕ	49
6.3 Variation of Density, Viscosity and Relaxation Time across the Interface	50
6.4 Weak Form	51
6.5 Finite-Element Approximation	52
6.6 Time Discretization	55
7 RESULTS	59
7.1 Leukocyte Deformation in the Absence of Adhesion Force	61
7.1.1 Composite-Drop Model	61
7.1.2 Drop-Rigid Particle Model	62
7.2 Lateral Migrations of Leukocyte in the Absence of Adhesion Force	64
7.3 Under Adhesive Force on the Channel Wall	65
7.3.1 Absence of pressure driven flow	66

TABLE OF CONTENTS
(Continued)

Chapter **Page**

7.3.2 Adhesion Potential Model: Motion near a Smooth Wall 67

7.3.3 Adhesion Potential model: Motion near a Wall Covered with Rigid Spheres 71

7.3.4 Kinetic Adhesion Model: Pressure Driven Flow 76

7.4 Comparison with Experimental Observations 82

8 CONCLUSIONS 87

9 FUTURE WORK 90

9.1 Cell Membrane Elasticity 90

9.2 Cytoplasm Modeled as Bingham Fluid (Yield-Stress Fluid) 91

9.3 Interactions between Blood Cells 91

LIST OF TABLES

Table **Page**

3.1 Parameters for the Two-Layered Leukocyte Models. 28

4.1 Parameter Values for the Kinetic Adhesion Model. 37

LIST OF FIGURES

Figure		Page
1.1	The different steps corresponding to the leukocyte extravasation	2
1.2	Blood as a suspension of blood cells	4
1.3	(a) Unstressed shape of red blood cell, (b) Average normal shape of red blood cell measured.	5
1.4	Different types of leukocytes.	6
2.1	(a). Linear; and (b) nonlinear small deformation, the dotted curves are initial shapes.	9
2.2	Continuous flipping motion of a viscoelastic membrane.	10
2.3	Tank treading of a RBC.	11
2.4	Orientation and deformation of RBC in shear flows.	17
3.1	Leukocytes in a passive state.	24
3.2	Drop-rigid particle model for leukocyte.	27
3.3	Composite-drop model for leukocyte.	28
4.1	Bonds formation between the ligands on the leukocyte surface and receptors on the substrate.	32
4.2	The adhesion force and the equilibrium bond density are shown as functions of the dimensionless bond stretching x'.	38
4.3	The bond density as a function of time when at t=0, x_m is suddenly increased from $(\lambda + l_{mv})$ to $1.01(\lambda + l_{mv})$. The new equilibrium value is approximately reached at $t=7\times10^{-6}$ s.	38
4.4	Bond density is shown as a function of time.	40
5.1	Schematic of a leukocyte in a pressure driven flow.	42
7.1	Leukocyte in a pressure driven flow – model set up.	59

LIST OF FIGURES

(CONTINUED)

Figure **Page**

7.2 Leukocyte deformation in the case of the compound-drop model at different distances from the wall. The shapes on the xz-mid plane through the leukocyte center are shown. (a) x=1.9, (b) x=2.425, (c) x=2.9, and (d) x=3.375 at time t=4.6. The deformation increases with decreasing gap between the leukocyte and the wall. Notice that both the leukocyte and the nucleus are deformed. The Reynolds number is 0.5. 61

7.3 Viscoelastic stresses contour on the xz-mid plane through the leukocyte center in the case of the compound-drop model at different distances from the wall is shown at (a) x=1.9, (b) x=2.425, (c) x=2.9, and (d) x=3.375 at time t=4.6. The Reynolds number is 0.5. 62

7.4 Leukocyte deformations in the case of the drop-rigid-particle model as a function of the distance from the wall. (a) x=1.9, (b) x=2.425, (c) x=2.9, and (d) x=3.375 at time t=4.6. The deformation increases with decreasing gap between the leukocyte and the wall. Since the nucleus is rigid, it does not deform. The Reynolds number is 0.5. 63

7.5 Deformation of a leukocyte represented by the drop-rigid-particle model at (a) t=0.82 and (b) t=5.25. The Reynolds number is 0.5. 63

7.6 Trajectories of leukocytes released from different positions within the channel. The Reynolds number is 0.5. 65

7.7 Deformation of a leukocyte near the wall due to the adhesion force in the absence of a pressure driven flow. The adhesion parameter is 50.0. Notice that the surface near the wall, as shown in the magnified view, is flat. (a) Kinetic model, t=0.6 s, (b) potential model, t=0.6. 67

7.8 Deformation of a leukocyte in the case of the drop-rigid-particle model due to shear forces while it moves towards the wall under the action of the adhesive force at (a) t=0.82 and (b) t=2.46. The Reynolds number is 0.5, Ca=0.167, De= 0.1 and Adh=50.0. 68

7.9 Leukocyte deformation in the case of the compound-drop model released close to the wall at (a) t=0.82, and (b) t=2.46, and (c) t=3.94. The right side view is also shown (d). The Reynolds number is 0.5, Ca=0.167, De= 0.1 and Adh=50.0. 70

7.10 Deformation of a leukocyte represented by the drop-rigid-particle model due to the shear forces while it moves towards the wall under the action of the adhesive force at (a) t=0.82 and (b) t=2.46. 71

LIST OF FIGURES
(CONTINUED)

Figure **Page**

7.11 Motion of a leukocyte near an uneven wall consisting of a layer of spheres. (a) The spheres are arranged on a rectangular lattice and initially the lower surface of the leukocyte is tangential to the x=1.1 plane. (b) Leukocyte dimensionless velocity as a function of time for Re=0.5, Ca=0.084, De= 0.1 and Adh=50.0..... 72

7.12 Leukocyte deformation in the case of the compound-drop model released close to an uneven wall consisting of a layer of rigid spheres. The parameters are Re=0.5, Ca=0.167, De= 0.1 and Adh=50.0. (a) t=0.82, (b) t=2.46, and (c) t=4.92. Both side and top views are shown. 74

7.13 Leukocyte deformationin the case of the compound-drop model released close to an uneven wall formed with a layer of rigid spheres. The parameters are the same as in Figure 7.12, except for the capillary number which is now Ca=0.084. 75

7.14 Leukocyte deformation in the case of the compound-drop model and the adhesion force given by the kinetic model at (a) t=0.6, (b) t=3, and (c) t=6, for a Reynolds number of Re=0.5, Ca=0.167, De= 0.1 and Adh=50.0 76

7.15 Leukocyte deformation in the case of the compound-drop model and the adhesion force given by the kinetic model. The parameters are selected so that the adhesion force is 100 times larger than for the case shown in Figure 7.14 at (a) t=0.6, (b) t=3 and (c) t=6. The parameters are the same as in Figure 7.14, except Adh=5000.0..... 77

7.16 Leukocyte sections on the domain mid-plane at different times for two values of the Reynolds number: (a) Re=0.25 and (b) Re=1..... 79

7.17 The time at which all bonds are broken, and the distance traveled in the flow direction at that time, are shown as functions of Re..... 80

7.18 Leukocyte sections on the domain mid-plane at different times for two values of the capillary number. The other parameters are held constant: Re=0.5, De=0.1 and Adh=50.0: (a) Ca=0.64, and (b) Ca=0.32. 81

7.19 The time and distance at which all bonds are broken, and the adhesion force becomes zero, are shown as a function of the capillary number, Ca. The Reynolds number is 0.5, De=0.1 and Adh=50.0..... 82

7.20 Parallel plate chamber system set up. The motion and deformation of the cells are observed and captured through the top plate by CCD camera. Chotard-Ghodsnia R et al. (2002) 83

LIST OF FIGURES
(CONTINUED)

Figure **Page**

7.21 Rolling of a leukocyte (inside circles) on the endothelium (view from the top). Other leukocytes are adhering on the substrate wall. Chotard-Ghodsnia R et al. (2002) 84

7.22 (a) Photographs extracted from a movie of a leukocyte (human neutrophil) rolling along the endothelial monolayer (in grey, phase contrast images). The mean velocity during this sequence is 3.0 μm/s. At the same time, the leukocyte shape changes and elongates. (b) Instantaneous leukocyte velocity with fluctuations 86

NOMENCLATURE

c – Polymer concentration in term of the zero shear viscosity

$\boldsymbol{D}$ – Symmetric part of velocity gradient, m/s^2

f_b – Single bond force, N

F_b – Total adhesion force per unit area, N/m^2

k_{r0} – Initial reverse reaction rate, 1/s

k_r – Reverse reaction rate, 1/s

k_{f0} – Initial forward reaction rate, m^2/s

k_f – Forward reaction rate, m^2/s

k_b – Boltzman constant, N.m/K

l_{mv} – Unstressed microvillus length, m

$\boldsymbol{n}$ – Outer normal vector

N_b – Bond density, $1/m^2$

N_{l0} – Initial ligands density per unit area, $1/m^2$

N_{r0} – Initial receptors density on the cell membrane per unit area, $1/m^2$

p – Pressure, N/m^2

R – Radius of the leukocyte, m

r – Radius of nucleus, m

t_c – Characteristic time, s

$\boldsymbol{u}$ – Velocity vector, m/s

$W(x)$– Adhesion potential, N.m

w – Adhesion strength, N.m

x_m – Bond length, m

x' – Dimensionless bond stretching length

x – Dimensionless distance from the channel wall

γ_{10} – Cortical tension, N/m

γ_{12} – Interfacial tension, N/m

ρ – Density, kg/m^3

η_0 – Plasma viscosity, Pa.s

η_1 – Viscosity of cytoplasm, Pa.s

η_2 – viscosity of nucleus (composite drop model), Pa.s

λ_r – relaxation time, s

λ – Equilibrium bond length, m

σ – Spring constant, N/m

σ_{ts} – Transition *s*pring constant, N/m

ϕ – Distance from the interface

CHAPTER 1

INTRODUCTION

1.1 Objective

A white blood cell (WBC), also called leukocyte, is a multicomponent system composed of a membrane, cytoplasm, and nucleus. Although the white blood cells constitute only a small fraction of blood cells, they play a very important role in the body's immune response. They do so either by fighting pathogens, viruses, or other cells (cancer cells for example), or by reaching the site of infection through the transendothelial migration. The endothelial monolayer itself is a part of the vessel wall. Endothelial cells are maintained in close contact with each other by a complex network of transmembrane adhesion proteins, especially cadherins. Diapedesis is the way leukocytes migrate through the endothelial junctions under the combined effects of signalisation, changes in the rheological properties and the cell-cell adhesion properties. As part of the migration process, circulating leukocytes must first adhere to the luminal surface of the endothelium. The interaction of leukocytes with the endothelial monolayer involves the sequential engagement of leukocytes and endothelial adhesion molecules. Early interactions are mediated by selectins and their carbohydrate ligands, which mediates leukocyte rolling. Then, leukocyte integrins and their ligands, including immunoglobulinlike intercellular adhesion molecules, mediate firm leukocyte adhesion. Inflammatory mediators like chemokines play a role in this firm adhesion by activating integrins on the leukocyte cell surface. Spreading follows, due to the ability of the cells to deform. Finally, after having reached the endothelial junctions, leukocytes undergo large

deformations to cross the interendothelial junctions, i.e. they deform rapidly, migrate through the endothelial monolayer (this process also called diapedesis) and reach the interstitial tissue. This series of events is illustrated in Figure 1.1.

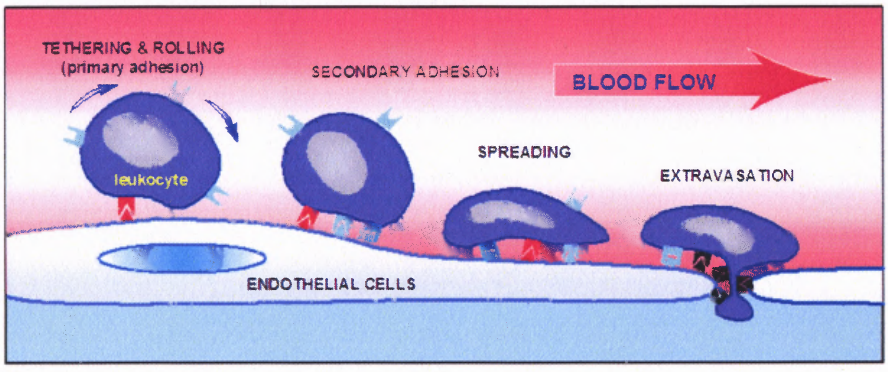

Figure 1.1 The different steps corresponding to the leukocyte extravasation.

The goal of this study is focused on the first phase of the above process, i.e., the study of the motion and deformation of leukocytes in small vessels and the investigation of conditions under which leukocytes can attach to the vessel wall and do not drift away. The leukocyte is assumed to be close to the endothelium layer. For this, the leukocyte is assumed to be already close to the endothelium. The factors, that cause leukocytes to get close to the endothelium in the first place, such as collisions with other cells, will not be studied. This study should also be helpful in improving the understanding of how cancerous cells are transported in the blood stream; in particular the effect of the flow rate, vessel size, as well as the influence of the transmural pressure might play a crucial role in cell-cell interactions which, in turn, is critical for the fate of these cancer cells (Burdick 2003). Indeed, it has been observed that the mechanisms by which cancer cells (Burdick 2003, Tözeren 1995, Haier 2001) migrate to and through the endothelium to

reach different tissues are similar to the ones used by leukocytes, although the adhesion molecules involved for the former are not all known yet.

It is necessary to understand the nature of blood where leukocytes are suspended and of the blood cells.

1.2 Background

Blood is an essential bio-fluid for life. The main function of the blood in circulation is to carry oxygen and nutrients through the body and to remove carbon dioxide and other waste products. Since other substances, such as hormones, white blood cells, and platelets, to sites where they are needed are also transported in blood. Blood is important also for hemostasis to prevent blood loss when the vascular system is damaged, as well as immune defense.

Essentially, blood is a suspension of blood cells, such as erythrocytes, leukocytes, platelets, in platelets in blood plasma as shown in Figure 1.2. Plasma is a mixture of water, sugar, fat, protein, and potassium and calcium salts. It also contains many chemicals that help form blood the clots necessary to stop bleeding. More than 92% of plasma is water. The viscosity of plasma alone is about 1.5 times that of water and it can be considered as a Newtonian fluid. Most of the cells in the field are mature Red Blood Cells (RBC's or erythrocytes). These cells are in a shape of biconcave disk about 7-8 μ m in diameter. Normal concentration of RBC's is about 4.5 to 5 million RBC's / mm^3. The large cells in nearly double the size of the RBC's (12 –15 μm), are one type of leukocyte, which are called neutrophils. Note that neutrophil contains segmented nucleus (3-5 segments is common) and the pale "pink" cytoplasm with very small "neutral" granules.

The normal concentration of WBC's in the peripherally circulating blood is about 5,000 - 10,000 WBC's / mm^3 and of that total, neutrophils will be about 55-65%.

The small isolated "dots" are platelets, also called thrombocytes. One microliter of normal human blood contains 300 Thousand platelets.

The understanding of the structure and dynamics of single cell is a prerequisite for the understanding of the rheology of blood.

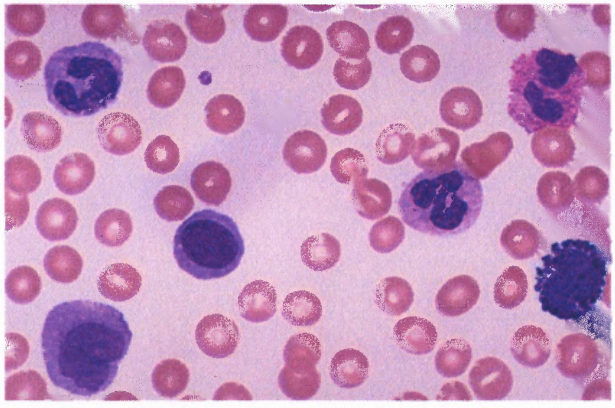

Figure 1.2 Blood as a suspension of blood cells.

A red blood cell (RBC), or erythrocyte, is a system of an elastic membrane containing a cytoplasm. It has no internal structure and lacks a nucleus. It consists of a Newtonian hemoglobin solution encapsulated by a bilayer membrane and a thin protein skeleton (Evans & Skalak 1980). The laminated membranes are responsible for highly non-Newtonian viscoelastic behavior of cells.

The role of Red blood cells (RBC) is to pick up oxygen when blood passes through the lungs and release it to the cells in the body. Each RBC consists of an elastic membrane and cytoplasm. Normal human RBC's in quiescent plasma assume a

biconcave discoid shape with average diameter of 8 μm, thickness of 2 μm, surface area of 140 μm^2, and volume of 90 μm^3 (Fung and Tong 1968, Evans and Fung 1972).

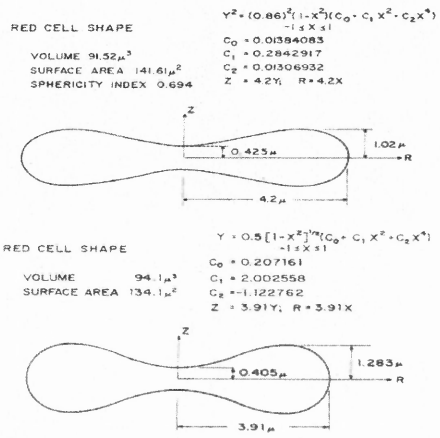

Figure 1.3 (a) Unstressed shape of red blood cell. (b) Average normal shape of red blood cell measured.

Source: Fung and Tong (1968); Evans and Fung (1972).

The surface area to volume ratio of the normal cell is 40% greater than that of a sphere with the same volume. Excess surface area not only improves the RBC's efficiency in loading and unloading solutions, but also allows it to deform easily. Shear forces can easily deform the membrane of the red blood cell while maintaining its local area nearly unchanged. This is due to the structure of the membrane, which is composed of a liquid bilayer, supported by a scaffolding of cytoskeletal proteins. Deformability affects RBC physiological function of oxygen transport and determines the hydrodynamic properties of whole blood.

Platelets are granular non-nucleated oval disks of fragments of cytoplasm with diameter around 2.5 μm. A platelet consists of two parts, an outer ground susbstance or shell occupying the greater part of the platelet and an inner part (core fluid) that contains

granules. Platelets play a major role in stop bleeding by accumulating at the injury sites and sticking together to form a clot that seals the cut in the blood vessels.

There are five different types of leukocytes: neutrophils (40% - 75% of all leukocytes in blood), lymphocytes (20% - 45%), monocytes (2% - 10%), eosinophils (1% - 6%), and basophils (less than 1%). Neutrophils, eosinophils, and basophils are known as granulocytes due to the presence of granules in their cytoplasm. Monocytes and lymphocytes are known as mononuclear cells as shown in Figure 1.4.

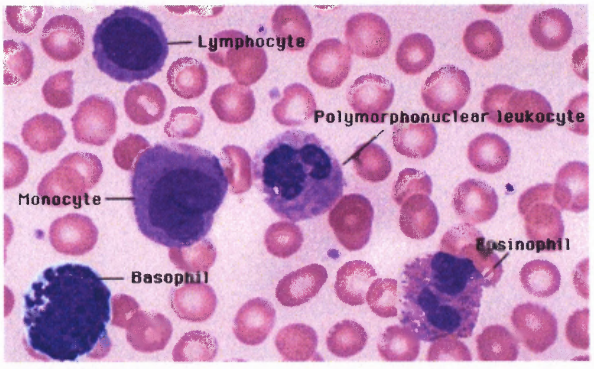

Figure 1.4 Different types of leukocytes.

A leukocyte is a complex system consisting of a membrane, which is folded or wrinkled under normal condition, cytoplasm, and nucleus. Leukocytes play a key role in the protecting the body from diseases causing by bacteria, virus, or parasites. To model the deformation and motion of leukocyte in blood flows, the rheological models of leukocyte are developed in Chapter 3.

CHAPTER 2

REVIEW OF PREVIOUS STUDIES ON DROPS DYNAMICS IN FLOWS

2.1 Free-Boundary Problems

The problems that concern with the motion of two or more contiguous immiscible fluids that are separated by an interface are known as free-boundary problems. Since the structure of a leukocyte is similar to that of a drop, the study of motions and deformations of leukocyte in flows is one application of free-boundary theories on blood cells dynamics. It is helpful to review the previous studies on deformation and migration of drops and capsules in flows.

2.2 Studies of Drops and Cells Deformation

In the study of drops and cells deformation in flows, one of the greatest difficulties is to track an unknown free boundary, namely the interface in the domain of interest. The interface shape determines the surface tension force and must be determined as a part of the solution. This phenomenon was revealed in many experimental observations. To physically model and solve this type of problems, analytical approaches were used firstly, but they are limited by the complexity of the governing equations. Recently, most of the free boundary problems are solved by using numerical methods, including finite element method, boundary element method, immersed boundary method These methods will be reviewed in the following sections. In this dissertation, level-set method combined with finite element method was used. More details of the computational approach adopted in this dissertation will be described in Chapterr 4.

2.2.1 Small Deformation Theories

The studies of neutrally buoyant drops in viscous shear flows were initiated by the early theoretical and experimental work of Taylor in 1932. In the limit of zero capillary number and infinite viscosity ratio, they obtained the internal and external velocity fields, and used these results to obtain the deformation and orientation of the drop to the first order in capillary number. Later studies of Cox (1969), Acrivos (1970, 1973), and Choi (2000) extended the theory to higher order in capillary number, and also when the base flow is transient.

Asymptotic theories describing small deformations of elastic capsules were developed by Barthes-Biesel and coworkers (Barthes-Biesel 1980, Barthes-Biesel & Rallison 1981, Barthes-Biesel & Sgaier 1985). The small deformations of capsules with spherical unstressed shapes enclosed by elastic or viscoelastic membranes were studied. The particle consists of a thin elastic spherical membrane enclosing an incompressible Newtonian viscous fluid. In particular, the nonlinear theory of large deformation of membrane shells was expanded up to second-order terms of ε. The motions of the internal liquid and of the suspending fluid are both described by Stokes equations.

The nondimensional equations governing incompressible Navier-Stokes flow inside and outside a capsule were given by

$$\nabla \cdot u = 0, \tag{2.1}$$

$$\left(\frac{\partial u}{\partial t} + u \cdot \nabla u\right) + \frac{\eta_i t_r}{\rho L_r^{\,2}}(\nabla p - \nabla^2 u) = 0, \tag{2.2}$$

$$\nabla \cdot u^* = 0, \tag{2.3}$$

$$\left(\frac{\partial u^*}{\partial t} + u^* \cdot \nabla u^*\right) + \frac{1}{\lambda}\frac{\eta_i t_r}{\rho L_r^{\,2}}(\nabla p - \nabla^2 u^*) = 0, \tag{2.4}$$

The following scalings are used to nondimensionalize time, length, velocity, pressure, and force:

$$t = \frac{\bar{t}}{t_r}, x = \frac{\bar{x}}{L_r}, u = \frac{\bar{u}t_r}{L_r}, p = \frac{\bar{p}t_r}{\eta}, F = \frac{\bar{F}L_r t_r}{\eta}, \tag{2.5}$$

where L_r and t_r are the chosen reference length and time, respectively, and η is the fluid viscosity.

On the deformed surface of the membrane, continuity of velocities was imposed together with dynamic equilibrium of viscous and elastic forces.

Since this problem is highly nonlinear, a regular perturbation solution was sought in the limiting case where the deviation from sphericity is small. A small parameter ε (the Capillary number) was defined as:

$$\varepsilon = \mu G d / Eh, \ \varepsilon << 1. \tag{2.6}$$

The deformation and orientation of the capsule were obtained explicitly in terms of the magnitude of the shear rate, the elastic coefficients of the membrane, the ratio of internal to external viscosities. The results in Figure 2.1 showed that the very viscous capsules were tilted towards the streamlines, whereas the less viscous particles were oriented at nearly 45 to the streamlines.

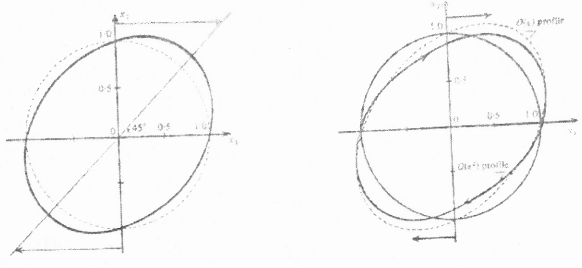

(a) (b)

Figure 2.1 (a). Linear; and (b) nonlinear small deformation, the dotted curves are initial shapes.
Source: Barthes-Biesel (1980)

The model also predicted the tank-treading motion of the membrane around the liquid contents as the consequence of a solid-body rotation superimposed upon a constant elastic deformation. Brunn (1983) extended these results to droplets enclosed by an elastic membrane with finite thickness. As to investigate the effect of the viscoelastic properties of the membrane on the deformation, the results of analytical work showed that with a purely viscous membrane, i.e., with infinite relaxation time, the capsule deforms into an ellipsoid and has continuous flipping motion, as shown in Figure 2.2.

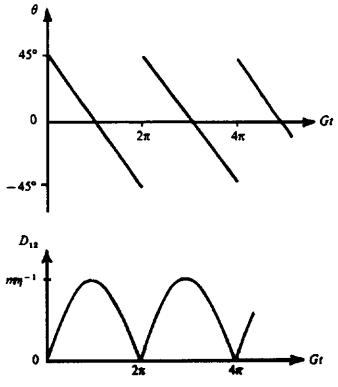

Figure 2.2 Continuous flipping motion of a viscoelastic membrane.
Source: Schmid-Schonbein and Wells (1969) and Goldsmith (1971).

The theoretical results by Schmid-Schonbein and Wells (1969) and Goldsmith (1971) in Figure 2.2 showed that when the membrane relaxation time was of the same order as the shear time, the particle reached a steady ellipsoidal shape which was oriented with respect to streamlines at an angle that varied between 45 and 0, and decreased with increasing shear rates. The deformation reaches a maximum value, which is consistent with the experimental observations of RBCs by Goldsmith and Marlow (1972), Keller & Skalak (1982), and Fischer (1978) as shown in Figure 2.3.

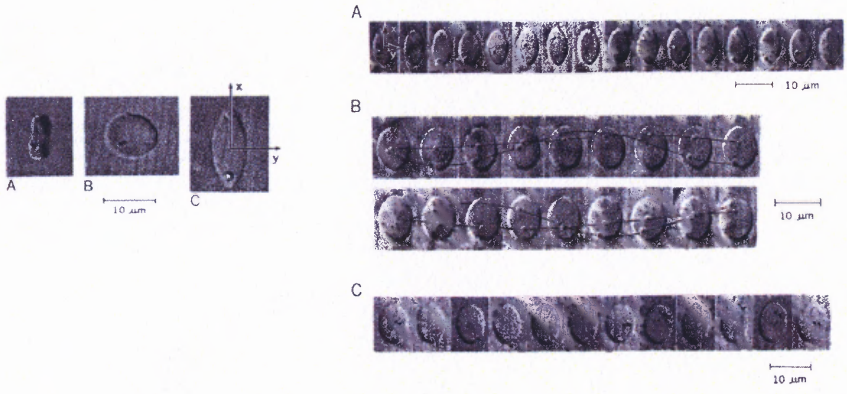

Figure2.3 Tank treading of a RBC.
Source: T. M. Fischer (1978).

This theory leads to the derivation of an asymptotic development of the large deformation theory of membrane shells. But the choice of an initial spherical geometry limits the applicability of this model to RBCs. For a diskoidal cell, the membrane incompressibility does not prevent large deformations, but determines the type of tank-treading motion. This theory is also limited by the small deformation assumption.

2.2.2 Experimental Studies of Drops and Cells Deformation.

Various researchers have published experimental results on the deformation and breakup drops undergoing extensional deformation. In extensional flows: the experiments were run using the four-roll mill. A detailed description of the four-roll mill and its operation was given by Bently & Leal (1986a, b). The strain rate ranges between 0.05 s^{-1} to $2s^{-1}$. The maximum deformation rate that can be obtained while keeping the capsules stationary is about 1 s^{-1}. At shear rates above 2 s^{-1}, the capsule oscillates about the stagnation point until it moves away from the central part of the flow. In shear flows, the studies of capsule motion were carried out in Coutte cell consisting of two counter-

rotating concentric cylinders. With the motors operating in the half-step mode, the range of shear rates can be obtained is 0.05 s^{-1} to 45 s^{-1}. The values of the viscosity ratio λ range from 0.004 to 0.08.

The shape and orientation of the capsule were measured. Compared the results with the predictions of small-deformation theory of Barthes-Biesel (1980), the data suggested that the membrane is viscoelastic, and the comparisons yielded values of the membrane elastic modulus and the membrane viscosity. These values also agreed well with the values deduced from other independent experiments.

Milliken and Leal (1991) studied viscoelastic drops in linear two-dimensional flows over a broad range of viscosity ratio. Elmendrop and Maalcke (1985) observed a linear relationship between drop deformation and shear rate for shear rates up to $6s^{-1}$, which correspond for the fluid system used to capillary number up to 1.10. Levitt and Macosko (1996) observed that the steady deformed drop looked like a spheroid with slightly sharper edges at small shear rate values, and like a cylinder with highly pointed ends when the shear rate was increased up to a value below the critical shear rate.

K.S.Chang & Olbricht (1993a, b) did the experimental studies on the deformation and breakup of a synthetic capsule in steady and unsteady simple shear flow or extensional flow. The capsule is liquid drop surrounded by a thin polymeric membrane. The diameter of the capsules ranges between 2 and 4 *mm,* and can be measured to $\pm 0.05mm$. Most capsules in this study have the membrane thickness of 7 μm. The capsule membrane was formed by an interfacial polymerization reaction on the surface of a liquid drop suspended in an immiscible liquid. Polydimethylsiloxane (silicon oil) was chosen as the drop liquid, which is Newtonian over a large range of shear rate and its

viscosity can be adjusted by mixing readily available grades of oil. The out-phase liquid is deionized water.

In shear flows when the flow-induced deformation becomes sufficiently large, the capsules break. Breakup begins at points near the principal strain axis of the undisturbed flow. It is correlated with local thinning of the membrane. In Extensional flow, for sufficiently large strain rates, the membrane exhibits strain hardening and a permanent change in its structure, both of which are reflected in the shape of the capsule.

The current understanding of the behavior of red blood cells in flows is greatly due to experimental observations of cells' deformation in unidirectional simple shear flow. Schmid-Schonbein and Wells (1969) and Goldsmith (1971) were the first to demonstrate that red blood cells in simple shear flow exhibit two types of motion: rotation like rigid particles at low shear rates, and a fluid drop-like motion and deformation at higher shear rates. In the latter type of motion the dimples of biconcave disk disappear and the cell assumes the shape of a prolate ellipsoid, while the membrane rotates like a tank tread around the cytoplasmic fluid. Subsequent research has shown that the ratio of viscosities between the suspending and cytoplasmic fluid may play an important role in demarcating the prevailing type of behavior, rotation versus deformation along a stationary axis. Membrane viscosity plays an important role in studies of tank-treading cells.

An essay of erythrocyte deformability has been devised employing an instrument called *rheoscope*. This is basically a counter-rotating cone-and-plate viscometer which subjects isolated erythrocytes to graded levels of fluid shear and measure the resulting deformation and motions, proposed by Sutera (1985). P.Mazeron (1997) made a Small-

Angle Light Scattering (SALS) study about the deformation of RBC under shear. The deformed cells were assumed to be three axis ellipsoids of constant volume for all shear stresses. SALS image of RBC under increasing shear stress in a Couette flow were obtained and accurate measurements of the angular positions of the principal axis have been carried out.

2.2.3 Numerical Approaches.

Choose an interface tracking method is the primary step to investigate this free-boundary problem numerically. There are several numerical approaches for tracking the interface between two immiscible liquids, e.g., the surface tracking method, volume of fluid method, the mapping method and the level set method. These methods have been used extensively to simulate viscous and inviscid two-phase flows.

2.2.3.1 Series-Expansion Technique. Large deformations of two-dimensional cylindrical capsules were studied by Rao (1994) by extending the perturbation equations to include terms up to sixth order of the perturbation (dimensionless shear-rate) parameter that is proportional to the shear rate. In order to handle the massive algebraic manipulations in this approach a symbolic manipulation program (REDUCE 3.1, Rand Corporation, Santa Monica, CA, 1983) is used, which both formulated the problems for the higher-order terms and solve them. Moderately large deformations (aspect ratios approaching 3) fall within the range of the analysis.

The solution for the flow field around an isolated capsule was used to calculate the apparent viscosity of a dilute suspension of flexible cylindrical particles, which

yielded the paradoxical result that the apparent viscosity decreases as the internal viscosity increases. This analysis is not valid for sufficiently large viscosity ratios.

2.2.3.2 Boundary Element Method. More general models of capsule deformation have been based on the boundary element method. By means of a *boundary- integral technique* (X.Z.Li & D. Barthes-Biesel 1988), it is possible to numerically determine the motion and large deformation of an axisymmetric capsule in an elongational flow.

The undisturbed velocity field was assumed to be a purely elongational flow given in the fixed reference frame by $v_1^{\infty} = 2x_1, v_2^{\infty} = -x_2, v_3^{\infty} = -x_3$. One advantage of using this method was that the geometric dimension of the problem was reduced by one, and the Stokes equations of the problem are reformulated as an integral equation which is solved on the interface. The dimension of the problem was thus reduced. Assuming that the particles Reynolds number is very small, the fluid motion may be described by the Stoke's equations. The two main parameters on which the deformation depends on are the capillary number which represents the ratio of viscous to elastic forces, and the ratio of the interior to exterior viscosity.

The capsule is surrounded by an infinitely thin elastic membrane having a *Mooney-Rivlin* constitutive behavior. The membrane which is very thin sheet of an isotropic elastic solid obeys a *Mooney* constitutive law. The influence of the initial geometry of the particle (*axisymmetric*: spherical, oblate, and prolate shapes) as well as that of the constitutive behavior of the membrane was studied.

A critical value of the non-dimensional shear rate (the capillary number) was found, beyond which the capsule continuously deforms and no steady state can be

reached. This is interpreted as the outset of burst. They predicted the burst of a capsule suspended in shear flow.

Pozrikidis (1995) used the boundary element method to obtain the time-dependent deformation of a capsule (for spherical and ellipsoidal) with an elastic membrane (quadratic approximation of a neo-Hookean membrane strain energy function) in simple shear flow in the regime of finite deformations. In the mathematical model they regarded the interface as a two-dimensional elastic medium. The velocity is required to be continuous across the interface, but the hydrodynamic surface force or traction undergoes a discontinuity $\Delta f = \sigma^{(1)} \cdot n - \sigma^{(2)} \cdot n$ that is balanced by the interfacial or membrane tensions. The boundary integral formulation for Stokes flow provided an integral equation for the velocity at the interface in terms of Δf.

$$u_j(x_0) = \frac{2}{1+\lambda} u_j^{\infty}(x_0) - \frac{1}{4\pi\mu}\frac{1}{\lambda+1}\int_S \Delta f_i(x) G_{ij}(x,x_o)\,dS(x) + \frac{\beta}{4\pi}\int_S u_i(x) T_{ijk}(x,x_0) n_k(x)\,dS(x) \tag{2.7}$$

where $u^{\infty} = (ky,0,0)$ is the incident shear flow, the point x_0 is located on the interface which is denoted by S, $\beta = (\lambda-1)/(\lambda+1)$, and

$$G_{ij}(x,x_0) = \frac{\delta_{ij}}{|\hat{x}|} + \frac{\hat{x}_i \hat{x}_j}{|\hat{x}|^3}, T_{ijk}(x,x_0) = -6\frac{\hat{x}_i \hat{x}_j \hat{x}_k}{|\hat{x}|^5} \text{ with } \hat{x} = x - x_0 \tag{2.8}$$

They obtained a critical deformation and shear rate, beyond which the rupture of the membrane would happen and no steady-state flow can be obtained. He also considered the rheology of dilute suspensions. A comparison made with the observations of K.S.Chang (1993) show good agreement.

The calculations of Pozrikidis (1995) for large shear rates were limited to relatively short time due to numerical problem, which was not enough to obtain steady state or go into the long time behavior.

Zhou and Pozrikidis (1995) used the boundary element method with interfacial tension based on surface tension with an incompressible constraint and neglecting the viscoelastic behavior as a model of the RBC membrane. Local area conservation was enforced through a kinematic condition which does not account for the extensional properties of the membrane.

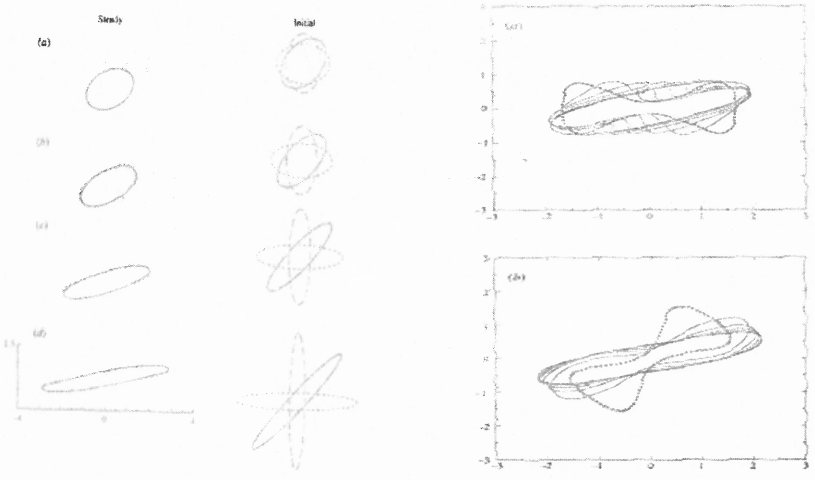

Figure 2.4 Orientation and deformation of RBC in shear flows
Source: Porikidis (1995)

The boundary element method has significantly improved to simulate capsules with hyperelastic membranes, and was able to solve moderate to large deformations of spherical and oblate shapes. Even with the improvements in the numerical method, numerical instability resulting from degradation of the grid and the neglect of bending resistance are problematic under conditions of high and low deformations, respectively.

The development of adaptive grid regeneration using the advancing-front method is the topic of a current investigation.

Y. Navot (1998) found out that the possibility of the steady-state flows were restricted by symmetry by means of analytical considerations. For a single spherically symmetric membrane, the steady-state shape exists and it depends on the shear stress by his numerical simulations. While for nonspherically symmetric membranes, there is no steady-state shape in general, but the changes of the shape can be periodic. This is an alternative explanation for the experimental results by Chang & Olbricht (1993). A dilute system of elastic membranes immersed in a liquid was studied, and he obtained a shear thinning behavior when the shear rate increases.

Pozrikidis (2001) studied the effect of membrane bending stiffness on the deformation of capsules in simple shear flow. He offered an alternative formulation for modeling the wall mechanics in Cartesian coordinates, relaxing the assumption of small deformation. An important restriction is the requirement that the resting shape has uniform curvature. For arbitrary resting shapes, the formulation in terms of surface curvilinear coordinates implemented either directly by force and torque balances or indirectly in terms of the principle of virtual displacements developed by Pedley and Heil appears to be the only alternative.

2.2.3.3 Immersed Boundary Method. The immersed boundary method was introduced by Peskin (1977) to simlulate blood flow in the heart. In C.D. Eggleton & Popel (1998)'s work, they used the immersed boundary method to simulate capsule deformation in which internal and external properties are equal, thus representing the flow of red blood cell ghosts. Unlike the BEM, fluid velocities are calculated in the

interior and exterior fluids at every time step. The methodology has been developed by Unverdi & Tryggvason (1992) for tracking the interface and accounting for the changes in fluid properties. Front tracking requires the solution of Poisson's equation on the entire fluid grid at every time step, thus it is more costly to implement. Haj-Hariri (1997) developed an adaptive grid refinement scheme in combination with a front tracking method to study thermocapillary motion of drops where the ratio of internal to external fluid viscosity ranged from 10^{-3} to 10^{1}.

The method has been validated for small deformations of an initially spherical capsule in simple shear flow for both neo-Hookean and the Evans-Skalak membrane models.

Evans and Skalak (1980) have developed a strain energy function for the RBC membrane which is fit to the deformation measurements for human RBCs. The *Evans-Skalak* membrane model that has been commonly used as the model for the RBC membrane is characterized by a *dilation modulus* that determines the resistance to local changes in area and an *extensional modulus* that determines the resistance to shearing stresses. Viscoelastic properties of the RBC membrane are not included in their model.

$$W = \frac{1}{4}B(\frac{1}{2}I_1^2 + I_1 - I_2) + \frac{1}{8}CI_2^2 = \frac{1}{4}B[2\Lambda_2^2 + 2\Lambda_2 + 1 - e^{2\Lambda_1}] + \frac{1}{8}C(e^{2\Lambda_2} - 1)^2 \qquad (2.9)$$

where $\Lambda_1 = \ln(\lambda_1\lambda_2) = \frac{1}{2}\ln(I_2+1)$, $\Lambda_2 = \frac{1}{2}I_1$, $I_1 = \lambda_1^2 + \lambda_2^2 - 2$, $I_2 = (\lambda_1\lambda_2)^2 - 1$, where B and C are material property constants whose values are deduced from experimental observations, or,

$$W_{RBC} = K_{RBC}(\lambda_1\lambda_2 - 1)^2 + \mu_{RBC}\left(\frac{\lambda_1^{\,2} + \lambda_2^{\,2}}{2\lambda_1^{\,2}\lambda_2^{\,2}} - 1\right), \qquad (2.10)$$

$$K_{RBC} = 500 dyn/cm, \mu_{RBC} = 6\times10^{-3} dyn/cm.$$

where λ_1, λ_2 are the principal strains using local in-plane curvilinear coordinates. The deformation is conveniently defined in terms of the principal extension ratio λ_1, λ_2 given by,

$$\lambda_1 = \frac{ds}{dS}; \lambda_2 = \frac{r}{R}. \tag{2.11}$$

The membrane which is very thin sheet of an isotropic elastic solid obeys a *Mooney* constitutive law.

As to initially oblate spheroidal capsules, it was showed that the RBC membrane exhibits *asymptotic behavior* as the ratio of the dilation modulus to the extensional modulus is increased, and the local area conservation was obtained.

To simulate more complex shapes, the bending stiffness must be included. Although the bending stiffness of the RBC is small, $k_c=10^{-12}$ erg (Mohandas 1994), it is necessary to smooth out the deformations and prevent buckling.

2.3 Lateral Migration of Drops and Particles

Blood flow is essentially a pressure driven flow. Besides the studies on the deformation of liquid drops and cells in flow above, previous researches also found that in pressure driven flows, drops or cells move in the direction which normal to the flow direction. This phenomenon is called lateral migration. To study the lateral migration of leukocyte in blood flows, it is helpful to review the previous studies on lateral migration of drops in the pressure driven flows. In the following sections, experimental, analytical and numerical studies on many types of liquid/solid particles and biological cells motion in pressure driven flows will be reviewed.

2.3.1 Experimental Studies

Goldsmith and Mason (1965) conducted experiments on migration of single rigid particle and deformable drops in a pressure driven flow in a tube at near-zero Reynolds number. They found that the axial migration of the drops was much appreciable than that of rigid particles. They found that in a tube flow, at low particle Reynolds number, the viscosity ratio $\lambda = \mu_i / \mu_o$, plays an important role. Especially for $\lambda = 10$, the drop migrated towards the wall, but for λ =50, the deformation was negligible, and there was no lateral migration. At high Reynolds number, the steady position was found to be between the wall and the centerline (r=1/2 R). The migration due to deformation can dominate that due to inertia. It was observed that liquid drops with small viscosity ratio (0.0002-0.02) migrated toward the tube axis in the flow of very low Reynolds number. Hiller and Lowalewski (1987) carried out the experiments of dilute suspension of droplets in a plane Poiseuille flow in the limit of creeping flow. They observed that for λ=0.1 the highest drop number density was at the centerline of the channel, while for λ=1 this position is somewhere between the wall and the center. Uijttewaal (1994) performed experiments with blood cells in two-dimensional Poiseuille flows, erythrocytes exhibit inertia-induced lateral migration at high Reynolds number and in a low viscosity medium. The migration is towards the center of the channel.

2.3.2 Analytical Studies

A comprehensive analysis of the migration of drops was performed by Chan and Leal (1979). They analytically studied the cross-stream migration of a single deformable drop in both Poiseuille and simple shear flows. The direction and magnitude of the migration

were calculated for various viscosity ratios of the two fluids. Their analysis assumes that the viscosity ratio $\lambda < O(1/Ca)$, where $Ca = \frac{\mu a}{\sigma}$ is the capillary number. They found that in Poiseulle flows, for $0.5 < \lambda < 10$, the motion of a drop is towards the centerline of the channel, while for all other values, the migration is toward the channel walls. The accuracy of the theory was confirmed by the experimental data.

2.3.3 Numerical Work

Recently, some numerical simulations of this problem were carried out by Zhou and Pozrikidis (1994), Couillette and Pozrikidis (1998) and Saeed and Tryggvason (2000). Zhou and Pozrikidis (1994) studied the dilute suspension of drops in Poiseuille flows. They found that drops with the same viscosity as the surrounding fluid migrate away from the wall of the channel. While for a single drop with a viscosity ratio of 10, if it is initially close to the centerline, it moves to the wall. But if it is initially close to the wall, it migrates toward the centerline. The viscosity ratio of $\lambda = 0.5$ is the lower critical value for which the direction of the migration changes. Their results generally agree with the theoretical work of Chan and Leal (1979). Couillette and Pozrikidis (1998) studied an array of large drops through a cylindrical tube. They assumed that the viscosity ratio as 1 and found that the drops migrate toward a position between the wall and the centerline. This case is similar as blood cells in flow through capillaries. Saeed and Tryggvason (2000) examined the dependence of drop migration on deformation, viscosity ratio, and Reynolds number. Their results showed that in the limit of a small Reynolds number (<1), for viscosity ratio 0.125, the drop moves toward the center of the channel, while for viscosity ratio 1 it moves away from the center until it is halted by the wall repulsion.

They also found that the deformation increases the migration rate. At high Reynolds number (5.50), the drop either moves to an equilibrium position between the centerline and the wall or it undergoes an oscillatory motion. They also found that the equilibrium position of three-dimensional drop is closed to that is predicted in their two-dimensional simulations.

In general, in the limit of small deformation, the migration depends on the viscosity ratio. For large deformations, the equilibrium position is the interplay of deformation and viscosity. At higher Reynolds numbers, Inertia force drives the drop toward the wall. This position moves to the centerline of the channel as the viscosity ratio decreases. At lower Reynolds numbers, deformation drives the drop migrate toward the centerline of the channel. The higher Re is, the closer the equilibrium position is to the wall of the channel.

CHAPTER 3

RHEOLOGICAL MODELS OF LEUKOCYTE

There are five different types of leukocytes: neutrophils, lymphocytes, monocytes, eosinophils, and basophils. These different types of leykocytes are of different sizes, with a nucleus or nuclei of different size and shape. Experimental observations however show that leukocytes behave similarly under comparable, relative deformation, but have different surface tension and viscous properties. Most of geometric and mechanical studies of leukocytes have focused on neutrophil because it is the most common leukocyte in blood, but the results with minor modification are generally applicable to all cells of leukocyte family. For the studies in this dissertation, neutrophil is selected to represent leukocyte.

A leukocyte can be observed in a passive state, where it is spherical, or in an active state, where it forms regions of polymerized protoplasm. The active state is initiated during diapedesis. Circulating leukocytes are usually in the passive state as shown in Figure 3.1, and this is the state concerned in this study.

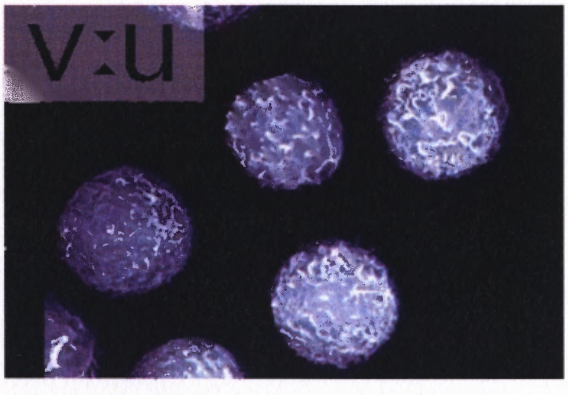

Figure 3.1 Leukocytes in a passive state.

The diameter of a circulating neutrophil is about 8 μm. A nucleus takes up about 21% of its volume. Neutrophil is enclosed by a ruffled membrane. The membrane surface contains folds, projections, and microvillis, which serve to increase its area. Osmotic swelling studies show that the apparent surface area of a neutrophil at lysis is 2.6 times of that under isotonic conditions. With the excess membrane area, the neutrophil can undergo large deformations. A tension in the cortical actin layer in the membrane keeps the shape of the cell spherical. This tension of 0.035dyn/cm is constant during small and moderate deformations of neutrophil, and thus the cell can be treated as a drop with a constant surface tension, brought up by Evan and Yeung (1989) and David Needham and Hochmuth (1992).

The rheological behavior of leukocytes has been extensively studied recently using the micropipette aspiration technique by Needham (1990) and Hochmuth (2000), Evans and Kukan (1984), and also using AFM (Zhang 2004). These techniques are combined with mathematical models where a leukocyte is modeled as a viscoelastic solid, or a drop of a Newtonian or viscoelastic fluid (Schmid-Schönbein 1981, Dong 1988, Drury 1999). These models, however, do not adequately explain experimental observations. In particular, experiments of Evans and Kukan (1984) showed that the neutrophil behaves more like a fluid than a solid, i.e., its rheology cannot be described by a viscoelastic solid model. Needham (1990) and Tran-Son-Tay (1991) reported that the response of neutrophils is non-Newtonian, i.e., and thus the neutrophil cannot be modeled as a Newtonian drop. Experimental data have shown that neutrophils or other cells can be modeled using the Maxwell model (Thoumine 1997, Canetta 1993). Tsai, Waugh (1993) found that the apparent viscosity of neutrophil's cytoplasm in cell micropipette aspiration

experiments was dependent on the aspiration pressure and proposed a power-law fluid model to describe passive neutrophil's non-Newtonian behavior at large deformations. Lomakina (2004) studied the dependence of neutrophil's mechanical behavior on contact area between the cell and substrate. Spillmann (2004) found the adhesion probability increased when increased the impingement force on the cell, since the force increased the contact area and the bond formation between b2-integrins on neutrophils and immobilized ICAM-1. Herrant (2005) found that the cortical tension increases with cellular area increases, but this change is much delayed in phagocytosis compared with aspiration. The recent numerical studies of Kan (1998), N'Dri (2005) and Khismatullin and Truskey (2005), based on a compound drop model, have been capable of qualitatively explaining the behavior of leukocytes observed in experiments. The compound drop model of a leukocyte consists of a spherical nucleus containing a core fluid which is surrounded by a thick layer of cytoplasm. The interfacial tensions act between both the nucleus and the cytoplasm, and between the cytoplasm and the blood plasma.

In this study leukocytes, which are the only blood cells with a nucleus, will be represented using two different two-layered models in which the outer layer represents the cytoplasm and the inner layer represents the nucleus. The two-layered models of leukocytes used here approximately represent neutrophils, although for simplicity the shape of the nucleus is assumed to be spherical.

3.1 Drop – Rigid Particle Model

The first model is a drop-rigid particle structure shown in Figure 3.2. In this two-layer structure, the outer layer is cytoplasm liquid that is Newtonian fluid, whereas the inner layer is a rigid particle that represents the nucleus of leukocyte. The nucleus takes 21% of the whole volume of the cell. Accordingly the thickness of the outer shell in this model is 2.7 μm. On the interface between cytoplasm and the surrounding fluid (plasma), a cortical tension is applied. This tension is similar as surface tension and it is of $3.0\times10^{-5}\,kg/m^2$ from the experimental data.

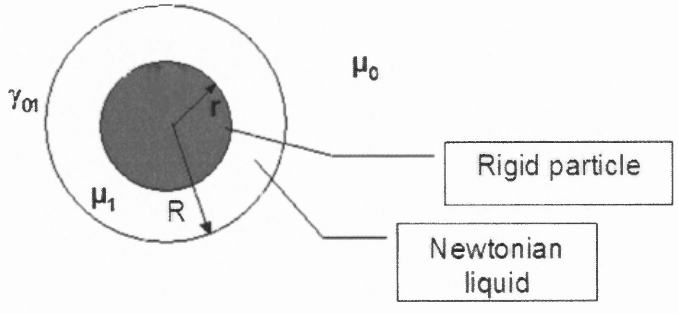

Figure 3.2 Drop-rigid particle model for leukocyte.

3.2 Composite Drop Model

The second model used for leukocyte is a composite drop model in Figure 3.3. In this model there are inner and outer interfaces: the inner interface is between core fluid and shell and the outer interface (leukocyte membrane) is between shell and extracellular fluid. The cortical tensions of $3.0\times10^{-5}\,kg/m^2$ are applied on both of the interfaces. The outer layer liquid of this model is considered to be Newtonian fluid, whereas the nucleus of the cell is regarded as a layer of viscoelastic liquid with different viscosity. These two layers both have higher viscosities than the extracellular fluid that is plasma.

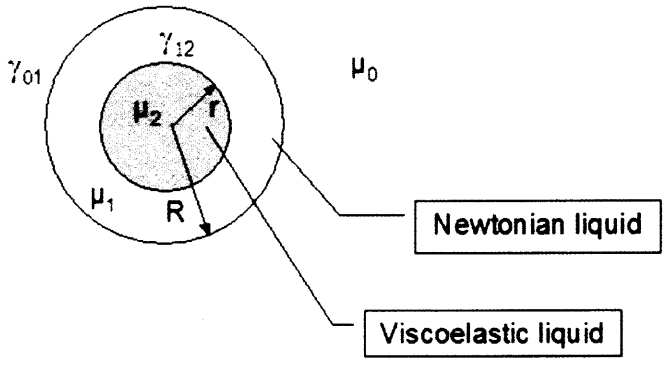

Figure 3.3 Composite-drop model for leukocyte.

Table 3.1 Parameters for the Two-Layered Leukocyte Models

Parameters	Values used
Radius, R	6.5 μm
Shell Thickness, R-r	2.7 μm
Cortical tension, γ_{10}	$3x10^{-5}$ N/m
Interfacial tension, γ_{12}	$3x10^{-5}$ N/m
Density, ρ	1000 kg/m^3
Viscosity of cytoplasm, η_1	35.28 Pa.s
Plasma viscosity, η_0	0.001 Pa.s
Viscosity ratio η_0 / η_1	0.01
*Viscosity ratio η_1 / η_2	0.35
*Relaxation time of nucleus, λ_r	0.1 s
*Viscosity of nucleus, η_2	100.0 Pa.s

Parameters marked with a star apply to the composite-drop model only.

The values of the parameters for the two previous models are given in Table 3.1. For the compound-drop model, three additional parameters are needed to describe the viscoelastic fluid in the nucleus. The other parameters are the same as for the drop-rigid particle model. The densities of the plasma and leukocyte are assumed to be equal, and thus the gravity plays no role in the dynamics.

CHAPTER 4

ADHESION MODELS

Under normal conditions, leukocytes are freely suspended in the blood stream. However, upon inflammation, the leukocytes that come close to the endothelial layer, as a result of the collisions with other blood cells and the expression or activation of adhesion molecules, can be captured. This latter process can be modeled by an adhesion force $\mathbf{F_b}$, which acts between the leukocytes and the endothelium. This force has a very short range and can result in the capture of leukocytes that come sufficiently close to the wall. Two models that are used to represent the adhesion force are described next.

4.1 Adhesion Potential

In the first model, introduced by Sukumaran and Seifert (2001), the adhesion potential of the leukocyte with a plane wall at $x = 0$ is assumed to be

$$W(x) = w\left(\frac{d_0}{x}\right)^2\left[\left(\frac{d_0}{x}\right)^2 - 2\right] \tag{4.1}$$

where w is the adhesion strength and $d_0 = 0.02R$ is a constant related to the cell radius R. The adhesion force resulting from this potential then takes the expression

$$F_b = -\frac{\partial W}{\partial x} = -\frac{4w}{x}\left(\frac{d_o}{x}\right)^2\left(-\left(\frac{d_o}{x}\right)^2 + 1\right) \tag{4.1'}$$

which becomes repulsive when $x < d_0$, is zero for $x = d_0$, and attractive for $x > d_0$. The force is maximal for $\sqrt{5/3}\, d_0$. For the parameters used, the force is maximum when x = ~0.17 μm. Also, notice that such a force depends only on x, and is time independent.

The reason for Sukumaran and Seifert to bring up this model and used it in cell adhesion calculations is because, any model with a strongly repulsive short range interaction and a weakly attractive long range interaction would be suitable. Numerically, the model chosen is most suitable because it minimizes numerical problems associated with sharply diverging forces at short length scales. In any specific physical situation, the exact form of the potential depends nonuniversally on the concrete experimental conditions. As long as this potential is repulsive on short length scales and attractive on long length scales, with a single minimum in between, the results derived in the present model will hold, at least qualitatively.

4.2 Kinetic Adhesion Model

For more accurate description of the adhesion force, the second adhesion model considered is the kinetic model proposed by Dembo (1988). In this model, the adhesion force between the cell membrane and the wall is assumed to arise due to the formation of bonds between the specific adhesion molecules on the cell membrane and the receptors on the substrate. A bond between the cell and the substrate is modeled as a Hookean spring, and the corresponding force f_b due to one bond is

$$f_b = \sigma(x_m - l_{mv} - \lambda) \tag{4.2}$$

where σ is the spring constant, x_m is the bond length, l_{mv} is the unstressed microvillus length, and λ is the equilibrium or unstretched bond length, and the total force per unit surface area between the cell and the substrate is

$$F_b = N_b f_b, \tag{4.3}$$

where N_b is the bond density per unit area. The bonds formation procedure is as illustrated in Figure 4.1.

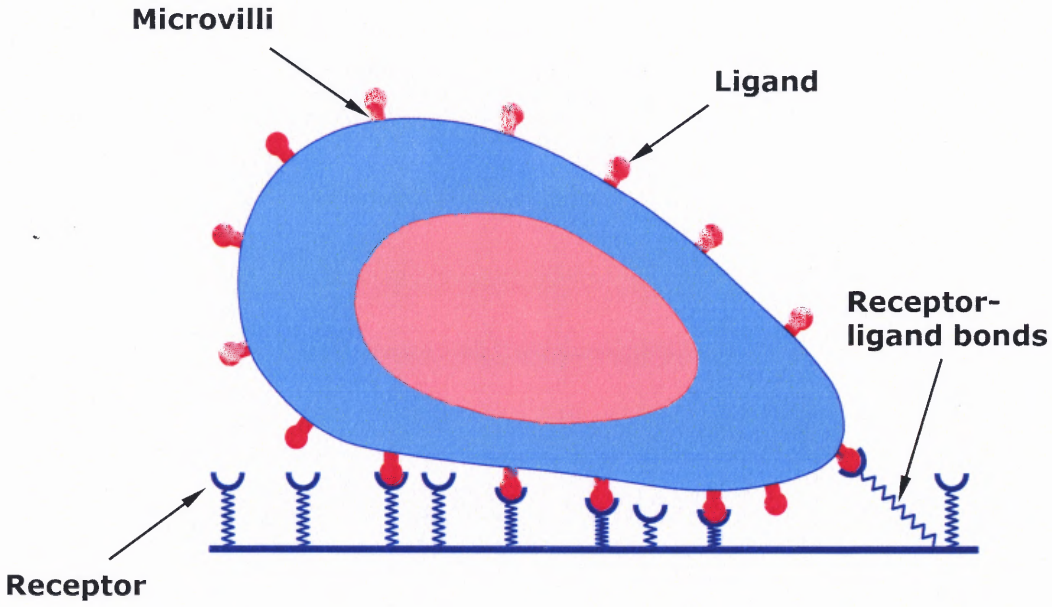

Figure 4.1 Bonds formation between the ligands on the leukocyte surface and receptors on the substrate.

To understand how to obtain the value of this bond density N_b, it is necessary to know the procedures of bonds formation between cells.

4.2.1 Rate Constants of Bonds Formation

The formation and breakage of cell-to-surface bonds at any position of the membrane is taken to be a reversible stochastic chemical rate process in Bell's model (1978). This process includes two steps for bond formation. In the first step, the receptors on the cell membrane and receptors on the endothelial cell diffuse into sufficiently close distance, and bonds form in the second step. This two-stepped procedure is described by following equation,

$$A+B \underset{d_-}{\overset{d_+}{\rightleftharpoons}} AB \underset{r_-}{\overset{r_+}{\rightleftharpoons}} C \tag{4.4}$$

where d_+, d_- are the rates of formation and dissolution of the mediate complex AB from reactants A and B, which are the receptors and ligands for the concerned case, and r_+, r_- are the rates of the formation and rupture of the bonds C from the complex AB.

In the current case, both reactants are attached on surfaces, separated by a distance R_{AB}, the encounter distance. It was shown in Dembo's (1978) model that,

$$d_+ = 2\pi[D(A)+D(B)] \tag{4.5}$$

$$d_- = 2[D(A)+D(B)]R_{AB}^{-2} \tag{4.6}$$

where $D(A)$, $D(B)$ are the diffusion constants for receptor motion on the membrane.

When the reaction reaches to an equilibrium status after some time, one can assume that $\frac{d[AB]}{dt} = 0$, then the overall reaction (4.4) becomes simplified as,

$$A+B \underset{k_-}{\overset{k_+}{\rightleftharpoons}} C \tag{4.7}$$

The relationship between the densities of reactants A,B and product C would be,

$$\frac{d[A]}{dt} = -k_+[A][B]+k_-[C] \tag{4.8}$$

and from balance of reaction one can obtain that,

$$\frac{d[AB]}{dt} = d_+[A][B]-d_-[AB]-r_+[AB]+r_-[C] = 0 \tag{4.9}$$

so the density of mediate complex AB can be expressed as

$$[AB] = \frac{d_+[A][B]+r_-[C]}{d_-+r_+} \tag{4.10}$$

For the first step of the diffusion, the density balance relationship is,

$$\frac{d[A]}{dt} = -d_+[A][B]+d_-[AB] \tag{4.11}$$

By substitute equation (4.11) into (4.9), obtain the relationship between the densities of reactants A,B and the final product C as,

$$\frac{d[A]}{dt} = \frac{-d_+ r_+ [A][B]}{d_- + r_+} + \frac{d_- r_- [C]}{d_- + r_+} \tag{4.12}$$

the rate constants of overall reaction are,

$$k_+ = \frac{d_+ r_+}{d_- + r_+}, \; k_- = \frac{d_- r_-}{d_- + r_+} \tag{4.13}$$

For bonds formation between the leukocyte's receptors and ligands on the endothelial cell, the reaction was described as a simple form in Dembo's model (1988) as,

$$N_f \underset{k_r}{\overset{k_f}{\rightleftharpoons}} N_b \tag{4.14}$$

where N_f and N_b are the surface density of free or unattached adhesion molecules and the density of consummated membrane-to-surface bridges respectively. k_r and k_f are the reverse and forward reaction rate coefficients, which have the same physical meaning as k_+, k_- in equation (4.13).

4.2.2 Analysis of the Kinetic Model for Bonds Formation

The time evolution of the bond density N_b is given by a kinetic equation which balances the formation and dissociation of bonds:

$$\frac{\partial N_b}{\partial t} = k_f (N_{l0} - N_b)(N_{r0} - N_b) - k_r N_b \tag{4.15}$$

where N_{l0} and N_{r0} are the initial ligands and receptors densities on the surface of the cell membrane.

The reverse and forward reaction rate coefficients k_r and k_f in (4.15) are given by:

$$k_r = k_{r0} \exp\left(\frac{(\sigma - \sigma_{is})(x_m - l_{m'} - \lambda)^2}{2k_b T} \right) \tag{4.16}$$

$$k_f = k_{f0} \exp\left(-\frac{\sigma_{ts}(x_m - l_{mv} - \lambda)^2}{2k_b T} \right) \tag{4.17}$$

where k_{r0} and k_{f0} are the equilibrium values of the reverse and forward reaction rates, σ and σ_{ts} are the spring and transition spring constants, k_b is the Boltzmann constant, and T is the temperature. The values of these parameters are listed in Table 4.1.

The equilibrium bond density N_{b0} reaches the maximum value N_{b0m} when the bond stretching $x = x_m - \lambda - l_{mv}$ is zero. For a given value of x_m, the equilibrium bond density N_{b0} satisfies the following quadratic equation, which is deduced by setting the time dependent term in (4.15) equal to zero

$$k_f (N_{l0} - N_{b0})(N_{r0} - N_{b0}) - k_r N_{b0} = 0 \tag{4.18}$$

and which admits two solutions:

$$N_{1,2} = \frac{(N_{r0} + N_{l0} + \frac{k_r}{k_f}) \pm D}{2} \tag{4.19}$$

where D is the discriminant of the quadratic equation, i.e.

$$D = \sqrt{(N_{r0} + N_{l0} + \frac{k_r}{k_f})^2 - 4N_{r0}N_{l0}} \tag{4.20}$$

It is easy to see that the larger solution N_1 leads to a value which is larger than the number of available bonds, and thus is not physically meaningful. Therefore, the only physical solution of (4.18) is N_2, and so the equilibrium bond density is

$$N_{b0} = \frac{(N_{r0} + N_{l0} + \frac{k_r}{k_f}) - D}{2} \tag{4.21}$$

For the parameter values listed in Table 4.1, the maximum value of the equilibrium bond density, which is deduced by setting $k_f = k_{f0}$ and $k_r = k_{r0}$, is $N_{b0m} = 1.5 \times 10^{14}\ \mathrm{m}^{-2}$.

Both the equilibrium bond density N_{b0} and the adhesion force vary with the distance between the cell membrane and the wall. In Figure 4.2 the adhesion force and bond density are shown as a function of the dimensionless bond stretching $x' = \frac{x}{\lambda + l_{mv}}.10^3$. Notice that when x' is approximately 48 the force reaches the maximum possible value. In terms of the dimensional variables, the force is maximum when $|x_m - \lambda - l_{mv}|$ = 14.9 nm, and the adhesion force is approximately zero when $|x_m - \lambda - l_{mv}|$ is greater than 27.9 nm. Therefore, the force is present only over the narrow distance range of 30 nm. Consequently, as discussed later, a cell can be captured only if it is located within the above range.

Table 4.1 Parameter Values for the Kinetic Adhesion Model

Parameters	Range	Values used in calculations
Initial ligand density on the surface, N_{l0}, m^{-2}	2.0 - 5.0 $\times 10^{14}$	1.5 $\times 10^{14}$
Initial receptors density on the cell membrane, N_{r0}, m^{-2}	2.0 - 5.0 $\times 10^{14}$	3.0 $\times 10^{14}$
Initial reverse reaction rate, k_{r0}, $1/s$	10^{-5} -10	10
Initial forward reaction rate, k_{f0}, m^2/s	10^{-18} -10^{-10}	10^{-10}
Spring constant, σ, N/m	0.00001 - 0.01	2 $\times 10^{-4}$
Transition spring constant, σ_{ts}, N/m	-0.005 - 0.0095	10^{-4}
Unstressed microvillus length, l_{mv}, m	3×10^{-7}	3×10^{-7}
Equilibrium bond length, λ, m	10^{-8} ~10^{-7}	10^{-8}
Thermal energy, k_bT, $N\cdot m$	3.8 ~ 4.3$\times10^{-21}$	4.28$\times10^{-21}$

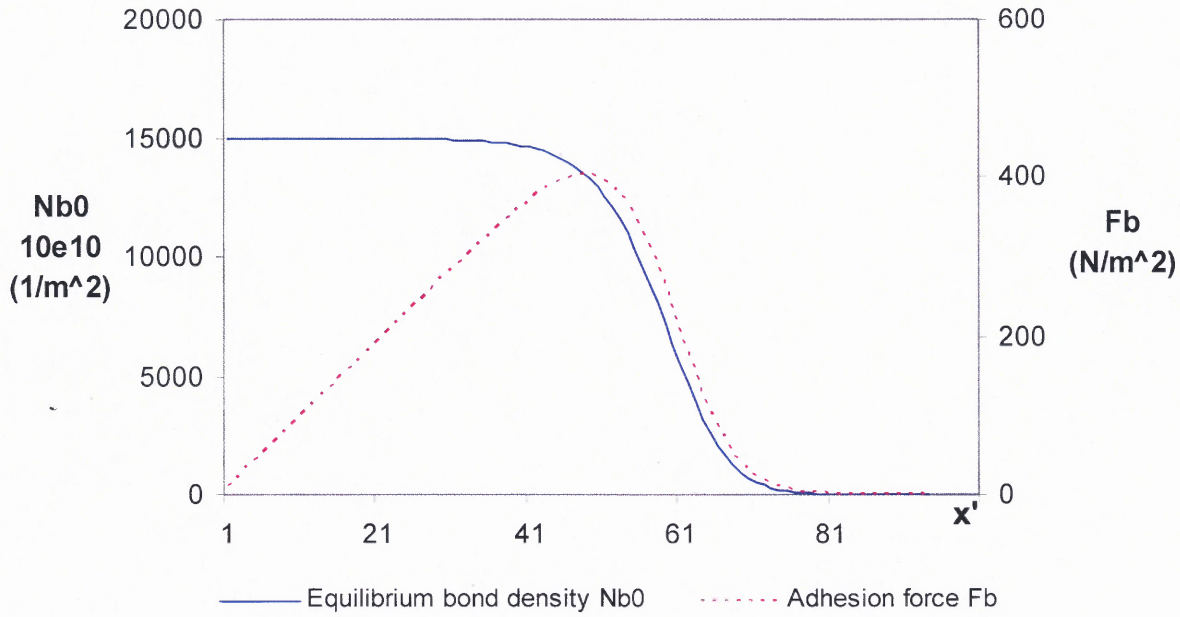

Figure 4.2 The adhesion force and the equilibrium bond density are shown as functions of the dimensionless bond stretching x'.

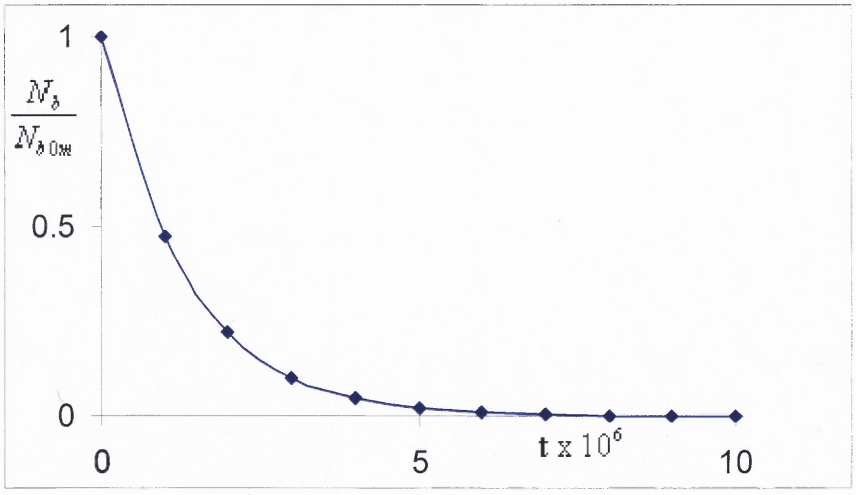

Figure 4.3 The bond density as a function of time when at t=0, x_m is suddenly increased from ($\lambda + l_{mv}$) to 1.01($\lambda + l_{mv}$). The new equilibrium value is approximately reached at t=7x10^{-6} s.

Next consider the time evolution of N_b when x_m is suddenly increased from (λ + l_{mv}) at t=0, to 1.01(λ + l_{mv}), which causes the bonds to break and the bond density to evolve to a new equilibrium value (see Figure 4.3). The bond density N_b in this case decays with time from N_{b0m} to a smaller value. The objective here is to determine the characteristic time over which the bond density evolves. This is relevant to the fluid dynamics problem because in a flow situation the distance between the cell wall and the endothelial monolayer changes with time. Clearly, if this characteristic time over which the new equilibrium value is reached is much smaller than the flow time scale, it is appropriate to assume in the fluid dynamics problem that the bond density is given by the steady solution of (4.15).

By integrating equation (4.15) analytically, it is easy to show that

$$N(t) = \frac{N_2 - \beta N_1 \exp(-t/\tau)}{1 - \beta \exp(-t/\tau)} \tag{4.22}$$

where N_1 and N_2 are the two roots defined in (4.19) and D is given by (4.20), $\tau = \frac{1}{k_f D}$, $\beta = \frac{\alpha - N_2}{\alpha - N_1} < 0$, and α is the initial bond density which, for the case considered, is N_{b0m}.

From (4.22) it is clear that as $t \to \infty$, obtain $N(t) = N_2$ as the solution for the new equilibrium state. Furthermore, it is interesting to notice that for all $t > 0$, one can have

$$N'(t) = \frac{(N_1 - N_2)\beta \exp(-t/\tau)}{\tau(1 - \beta \exp(-t/\tau))^2} < 0. \tag{4.23}$$

A plot of the bond density N_b as a function of time t is shown in Figure 4. Then define the characteristic time t_c to be,

$$t_c = \frac{\tau(N_1 - N_2)}{(N_1 - \alpha)} = \frac{1}{k_f(N_1 - \alpha)} \tag{4.24}$$

From the above expression, it is deduced that while t_c depends on k_f, k_r, N_{r0}, N_{l0}, it is independent of σ_{ts}, σ.

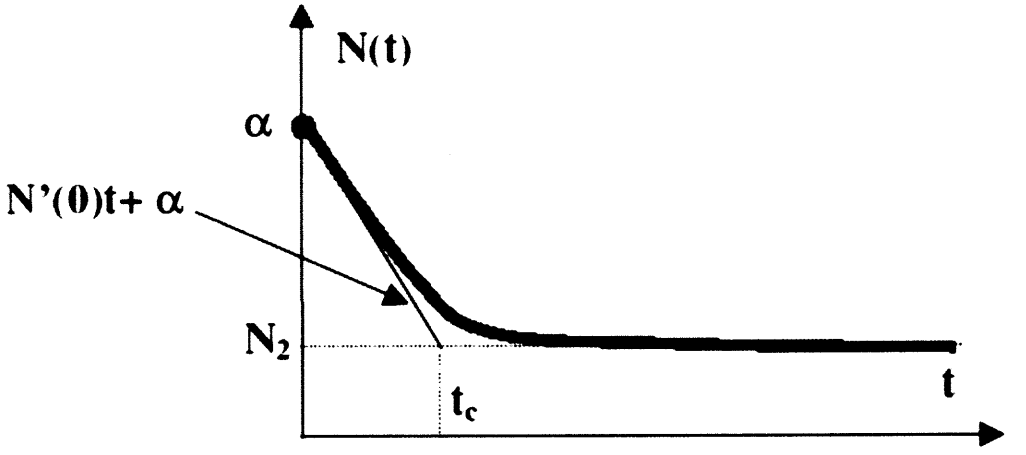

Figure 4.4 Bond density is shown as a function of time.

For the parameter values listed in Table 4.1, the characteristic time t_c given by equation (4.24) is $O(10^{-4})$ s. If the shear rate is between 10 and 100 s^{-1}, the characteristic flow time will be between 0.01~0.1 s. It is worth noticing that only when these two time scales are comparable it is necessary to consider the time evolution of the bond density for computing the adhesion force. If this is not the case, which happens for the parameter values selected in this study, it is appropriate to assume in the fluid dynamics problem that the bond density is equal to the equilibrium value for that particular bond length. The adhesion force, in this case, depends only on the distance between the cell surface and the wall, which is also the case for the potential model. The two models are similar in this sense, except that for the kinetic model the force range is much shorter. The dependence of the adhesion force on the distance from the wall for the two models, however, is different. Also, notice that the characteristic time scales for the kinetic and fluid

dynamics problems can be made comparable by selecting a different set of parameters in the kinetic model.

CHAPTER 5

GOVERNING EQUATIONS

5.1 Problem Description

The motion of a deformable leukocyte or cancer cell through a capillary or blood vessel is studied. The problem is as illustrated in Figure 5.1. The domain was defined similar as in the experiments setup of Chotard-Ghodsnia (2002). They used a parallel-plate flow chamber to simulate leukocyte and tumor cell extravasation under flow conditions. A cell monolayer is cultured on the lower plate of the flow chamber to model the endothelial barrier. Leukocytes and circulating tumor cells can be introduced into the flow channel under a well-defined flow field and tumor cell adhesion to endothelial monolayer can be followed *in situ*.

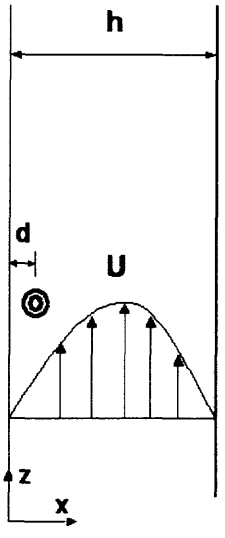

Figure 5.1 Schematic of a leukocyte in a pressure driven flow.

The simulation domain is a three-dimensional parallel plate channel. The distance between upper and lower walls of the channel h is $50\,\mu m$, and the width of channel is

$37\,\mu m$. Since blood flow through blood vessel is a type of pressure driven flow. The pressure gradient between the inlet and outlet of the channel is $\frac{dp}{dz}$. The velocity profile of pressure driven flow is $w(x) = \frac{1}{2\mu}\frac{dp}{dz}x(x-h)$. Leukocyte was initially released at a close distance x from the channel left wall. Under normal conditions, leukocyte is freely suspended in blood plasma; while under certain physiological conditions (flow rate, etc.), the cell begins to adhere to the endothelium, and eventually rolls, deforms and extravasates through the endothelium. Firstly it is studied without the existence of the adhesion force on the channel. Then the adhesive force is also included in the model.

5.2 Governing Equations

The domain containing the viscoelastic fluid and a drop (or a bubble) is denoted by Ω, and the domain boundary by Γ. The upstream part of Γ will be denoted by Γ^-. The governing equations for the two fluid systems are:

$$\nabla.\mathbf{u} = 0 \tag{5.1}$$

$$\rho\left[\frac{\partial \mathbf{u}}{\partial t} + \mathbf{u}.\nabla\mathbf{u}\right] = \rho\mathbf{g} - \nabla p + \nabla.\left(\frac{c\eta_s}{\lambda_r}\mathbf{A}\right) + \nabla.(2\eta_s\mathbf{D}) +$$

$$+\gamma\,\kappa\,\delta(\phi)\,\mathbf{n} + F_b L\delta(\phi)\,\mathbf{n} \tag{5.2}$$

$$\mathbf{u} = \mathbf{u}_L \text{ on } \Gamma, \tag{5.3}$$

with the evolution of the configuration tensor **A** given by

$$\frac{\partial \mathbf{A}}{\partial t} + \mathbf{u}.\nabla\mathbf{A} = \mathbf{A}.\nabla\mathbf{u} + \nabla\mathbf{u}^T.\mathbf{A} - \frac{1}{\lambda_r}(\mathbf{A} - \mathbf{I}), \tag{5.4}$$

$$\mathbf{A} = \mathbf{A}_L \qquad \text{on } \Gamma^-.$$

Here **u** is the velocity, p is the pressure, η_s is the solvent viscosity, ρ is the density, F_b is the adhesion force that acts along the interface. **D** is the symmetric part of the velocity gradient tensor, c is a measure of polymer concentration in terms of the zero shear viscosity, **n** is the outer normal, γ is the surface tension, κ is the surface curvature, ϕ is the distance from the interface, and λ_r is the relaxation time of the viscoelastic fluid, $\lambda_r/(1+c)$ is the retardation time, **n** is the outer normal, γ is the surface tension, κ is the surface curvature, ϕ is the level set function which is defined to be the distance from the interface and δ is the delta function. The polymer concentration parameter c is measure of the fluid's viscoelasticity; if it is zero the fluid is Newtonian and the viscoelasticity increases with increasing c. It is defined in terms of the fractional contribution to viscosity that arises due to viscoelasticity. That is, the polymer contribution to the viscosity is $\eta_p = c\eta_S$, and the zero shear viscosity of the fluid is $\eta_o = \eta_s + \eta_p$, where $\eta_p = c$ η_s is the polymer contribution to viscosity. The fluid retardation time is equal to $\frac{\lambda}{1+c}$.

The surface tension force acts only along the interface, i.e., for $\phi = 0$.

The cell interface is tracked using the level set ϕ which is convected according to the local velocity, i.e.,

$$\frac{\partial \phi}{\partial t} + \mathbf{u}.\nabla\phi = 0\,. \tag{5.5}$$

The remaining details of the numerical scheme used to advect the level set are described in Chapter 6.

The nucleus in the compound-drop model of leukocytes is assumed to be a viscoelastic liquid and modeled using the Oldroyd-B model. The evolution of the viscoelastic stresses, in terms of the configuration tensor **A**, is given by

$$\frac{\partial \mathbf{A}}{\partial t}+\mathbf{u}\cdot\nabla\mathbf{A}=\mathbf{A}\cdot\nabla\mathbf{u}+\nabla\mathbf{u}^{T}\cdot\mathbf{A}-\frac{1}{\lambda_r}(\mathbf{A}-\mathbf{I}) \tag{5.6}$$

Here **u** is the velocity, p is the pressure, η_s is the solvent viscosity, ρ is the density, **D** is the symmetric part of the velocity gradient tensor, c is the polymer concentration parameter, λ_r is the relaxation time of the viscoelastic fluid, $\lambda_r/(1+c)$ is the retardation time, **n** is the outer normal, γ is the surface tension, κ is the surface curvature, ϕ is the level set function which is defined to be the distance from the interface and δ is the delta function. The polymer concentration parameter c is a measure of the fluid's viscoelasticity; if it is zero the fluid is Newtonian and the viscoelasticity increases with increasing c. It is defined in terms of the fractional contribution to viscosity that arises due to viscoelasticity. That is, the polymer contribution to the viscosity is $\eta_p = c\eta_S$, and the zero shear viscosity of the fluid is $\eta_o = \eta_s + \eta_p$.

The particle velocity **U** and angular velocity $\boldsymbol{\omega}$ are governed by

$$\begin{aligned} M\frac{d\mathbf{U}}{dt} &= \mathbf{F} \\ \frac{\mathrm{d}(\mathbf{I}_P\,\boldsymbol{\omega})}{\mathrm{dt}} &= \mathbf{T} \\ \mathbf{U}|_{t=0} &= \mathbf{U}_0 \\ \boldsymbol{\omega}|_{t=0} &= \boldsymbol{\omega}_0 \end{aligned} \tag{5.7}$$

where M and $\mathbf{I}_P$ are the mass and moment of inertia of the particle, and the particle density is denoted by ρ_P. The force **F** acting on a particle in the above equations is

$$\mathbf{F} = \oint(-p\mathbf{I}+\boldsymbol{\sigma}).\mathbf{n}\,dA \tag{5.8}$$

where $\boldsymbol{\sigma} = 2\eta_S\mathbf{D}$ is the extra stress tensor and the integral is over the particle surface. Similarly, the torque **T** acting on the particle takes the expression

$$\mathbf{T} = \oint(\mathbf{x}-\mathbf{X})\times\left[(-p\mathbf{I}+\boldsymbol{\sigma}).\mathbf{n}\right]dA \tag{5.9}$$

where **X** is the center of the particle.

5.3 Nondimensionlization of the Governing Equations

The equations governing the fluid and leukocyte motions are nondimensionalized by assuming that the characteristic length, velocity, time and stress scales are R, U, R/U and $\eta_0 U/R$, respectively. Here R is the leukocyte radius, η_0 is the plasma viscosity, and U is the centerline velocity of the undisturbed pressure driven flow. The nondimensional equations, after using the same symbols for the dimensionless variables, take the expressions:

$$\nabla\cdot\mathbf{u}=0$$

$$\frac{d\mathbf{u}}{dt} = -\nabla p + \frac{1}{De\ \mathrm{Re}}\nabla.(c\mathbf{A}) + \frac{1}{\mathrm{Re}}\nabla.(2\eta_s'\mathbf{D}) + \frac{1}{\mathrm{Re}\ Ca}\delta(\phi)\mathbf{n} + \frac{\mathbf{F_b}}{\rho U^2}\delta(\phi)$$

$$\frac{\partial\mathbf{A}}{\partial t}+\mathbf{u}\cdot\nabla\mathbf{A}=\mathbf{A}\cdot\nabla\mathbf{u}+\nabla\mathbf{u}^{\mathrm{T}}\cdot\mathbf{A}-\frac{1}{\mathrm{De}}(\mathbf{A}-\mathbf{I}) \tag{5.10}$$

The above dimensionless equations contain the following parameters:

Reynolds number $$\mathrm{Re}=\frac{\rho_0 UR}{\eta_0} \tag{5.11}$$

Capillary number $$Ca=\frac{U\eta_0}{\gamma} \tag{5.12}$$

Weber number $$We=\frac{\rho_0 U^2 R}{\gamma} \tag{5.13}$$

Viscosity ratios $$\lambda_1=\frac{\eta_0}{\eta_1},\lambda_2=\frac{\eta_0}{\eta_2} \tag{5.14}$$

Adhesion number $$Adh=\frac{F_b}{\rho_0 U^2} \tag{5.15}$$

Dimensionless viscosity $\eta_s'=\eta_s/\eta_0$. (5.16)

For most cases reported, the dimensionless parameters are Re=0.5, Ca=0.167, De= 0.1 and Adh=50.0. For some cases Re, Ca and Adh are varied.

The role of these dimensionless parameters (Re, Ca, Adh and viscosity ratio) on the leukocyte's motion and deformation in blood flows will be investigated in Chapter 6. Studies of these parameters can help to find out and determine the critical conditions under which the leukocyte can remain attached on the blood vessel wall.

In the adopted method the governing equations are solved everywhere simultaneously, i.e., both inside and outside the drops/bubbles in the domain. In this sense, this approach is different from the methods which decoupled and solved the flow fields inside and outside the drop separately. In a decoupled approach one must apply suitable boundary conditions at the interface, i.e., impose the continuity of velocity and shear stress across the interface, and the jump in the normal stress across the interface is set to be equal to the surface tension force. Also note that since in presnet approach the governing equations are solved in a coupled manner, the method is stable and allows relatively larger time steps to be taken. The details of the numerical approaches used for solving the above governing equations will be described in Chapter 6.

CHAPTER 6

NUMERICAL APPROACH

A code based on the finite element method (Singh 1993), with features described in (Glowinski 1998, Singh 2000, Singh 2005), is used for solving the time dependent problem for the deformation of a leukocyte in a pressure driven flow. Here, the governing equations are solved simultaneously everywhere, i.e., both inside and outside the leukocyte in the computational domain, and the Marchuk-Yanenko operator-splitting technique is used to decouple the difficulties associated with the incompressibility constraint, the nonlinear convection term, the interface motion, the enforcement of the rigid body motion in case of a rigid nucleus, and the viscoelastic term (Glowinski 1998). The first problem is solved by means of a conjugate gradient (CG) method (Glowinski 1998, Singh 2000) and the second problem is dealt with using a least square conjugate gradient method (Glowinski 1998, Singh 2000). The third problem consists of the advection of the level set function ϕ, which is solved using a third order upwinding scheme (Pillapakkam 2001). The advected function ϕ is then reinitialized to be a distance function, which, as noted in (Sussman 1994), is essential for ensuring that the scheme accurately conserves mass. The rigid body constraint inside the rigid nucleus is enforced using the distributed Lagrange multiplier method (Glowinski 1998, Singh 2000). For all results reported in this study, the mass change was less than one percent. The adhesion force between the wall and the leukocyte is treated as a body force. The details of the numerical scheme used are described in the following sections.

6.1 Level-Set Method

The key idea in the level set method is to define a scalar variable ϕ equal to the distance from the interface and set the zero level set of ϕ as the interface. The level set ϕ is convected according to the local velocity, i.e.,

$$\frac{\partial \phi}{\partial t} + \mathbf{u}.\nabla\phi = 0 \tag{6.1}$$

Clearly, if ϕ satisfies the above equation and $\phi = 0$ at $t = 0$ along the interface, the zero level set of ϕ marks the interface for all $t > 0$. In this implementation, the distance function ϕ is considered positive for the region outside the drop and negative for the region inside. When ϕ is convected according to (6.1) it will not remain the distance function for the points away from the interface, and therefore, as discussed below, it must be reinitialized to be a distance function.

6.2 Reinitialization of ϕ

The level set function ϕ is reinitialized to be a distance function after each time step by solving the following equation obtained by Sussman (1994), to the steady state

$$\frac{\partial \phi}{\partial t} + \mathbf{w}.\nabla\phi = S(\phi_0) \tag{6.2}$$

where ϕ_0 is the distribution to be reinitialized and

$$\mathbf{w} = S(\phi_0)\frac{\nabla\phi}{|\nabla\phi|}.$$

Here $S(\phi_0)$ is the sign function, i.e., $S(\phi_0) = 1$ if $\phi_0 > 0$ and $S(\phi_0) = -1$ if $\phi_0 < 0$. In order to avoid discontinuities, in this code the following smoothed sign function is used

$$S(\phi_0) = \frac{\phi_0}{\sqrt{\phi_0^2 + h^2}}.$$

Equation (6.2) is a first order partial hyperbolic differential equation which is solved using a positive only upwinding scheme described by Sussman (1994). Clearly, the characteristics of (6.2) point in the direction of **w**. Also note that for the points outside the drop **w** points away from the drop and for the points inside the drop it points inwards. Thus, (6.2) can be solved by specifying the boundary condition $\phi = \phi_0$ at the two-fluid interface $\phi = 0$.

6.3 Variation of Density, Viscosity and Relaxation Time across the Interface

In the finite element scheme used in computation the fluid viscosity is assumed to take a jump across the interface, i.e,

$$\eta = \begin{cases} \eta_d & \text{if } \phi < 0 \\ 0.5(\eta_d + \eta_L) & \text{if } \phi = 0\, \phi < 0 \\ \eta_L & \text{if } \phi > 0 \end{cases} \tag{6.3}$$

Here η_d and η_L are the viscosities of the fluids inside and outside the drop, respectively. In other words, the nodes that are inside the drop have the drop viscosity and the nodes that are outside have the fluid viscosity. The fluid density, on the other hand, is assumed to vary smoothly across the interface,

$$\rho = \begin{cases} \rho_d & \text{if } \phi < -h \\ \rho_L & \text{if } \phi > h \\ 0.5(\rho_d + \rho_L) - 0.5(\rho_d - \rho_L) \cdot \sin\left(\dfrac{\pi\phi}{2h}\right) & \text{otherwise} \end{cases} \tag{6.4}$$

where h is equal to one and half times the element size, and ρ_d and ρ_L are the densities of the fluids inside and outside the drop, respectively. This smoothing of the density is similar to that in Sussman (1994), and is needed for avoiding numerical instabilities for relatively large density ratios ρ_d/ρ_L. The fluid relaxation time is assumed to jump across the interface

$$\lambda_r = \begin{cases} \lambda_d & \text{if } \phi < 0 \\ 0.5(\lambda_d + \lambda_L) & \text{if } \phi = 0 \\ \lambda_L & \text{if } \phi > 0 \end{cases} \tag{6.5}$$

Here λ_d and λ_L are the relaxation times of the fluids inside and outside the drop, respectively. If the fluid inside (or outside) the drop is Newtonian its relaxation time is set to zero. A relaxation time of zero ensures that the fluid relaxes instantaneously and thus behaves like a Newtonian fluid.

The surface tension force is smoothed and acts on the elements for which ϕ is smaller than h using the approach described in Sussman (1994). This approach requires that ϕ be maintained as a distance function, which is done in the depicted implementation by reinitializing ϕ after each time step.

6.4 Weak Form

The weak form of the governing equations is obtained by multiplying equations (5.3), (5.4), (5.6) and (6.1) by the test functions, and integrating the second order term by parts. This is a straightforward procedure with an additional complication that the fluid properties are not constant in the domain. Furthermore, since the fluid is viscoelastic, it's also needed to solve the constitutive equation (5.6) along with the momentum and continuity equations. In

obtaining this weak form, the hydrodynamic stresses acting at the interface are completely eliminated.

To state the combined weak form for the equation of motion the following spaces are needed:

$$W_u = \{\mathbf{v} \in H^1(\Omega)^2 \mid \mathbf{v} = \mathbf{u}_\Gamma(t) \quad \text{on} \quad \Gamma\},$$

$$W_{u0} = \{\mathbf{v} \mid \mathbf{v} \in H^1(\Omega)^2 \text{ and } \quad \mathbf{v} = 0 \text{ on } \Gamma\}$$

$$W_A = \{\mathbf{A} \in H^1(\Omega)^3 \mid \mathbf{A} = \mathbf{A}_L(t) \quad \text{on} \quad \Gamma^-\},$$

$$W_{A0} = \{\mathbf{A} \in H^1(\Omega)^3 \mid \mathbf{A} = 0 \quad \text{on} \quad \Gamma^-\},$$

$$W_\phi = \{\phi \in H^1(\Omega) \mid \phi = \phi_0(t) \quad \text{on} \quad \Gamma^-\},$$

$$W_{\phi 0} = \{\phi \in H^1(\Omega) \mid \phi = 0 \quad \text{on} \quad \Gamma^-\},$$

$$L_0^2(\Omega) = \{q \in L^2(\Omega) \mid \int_\Omega q \, dx = 0\} \tag{6.6}$$

where Γ^- is the upstream part of Γ. It is easy to show that the following weak formulation of the problem holds for the two-phase system:

For a.e. t>0, find $\mathbf{u} \in W_u$, $\mathbf{A} \in W_A$, $p \in L_0^2(\Omega)$ and $\phi \in W_\phi$, satisfying

$$\int_\Omega \rho\left(\frac{d\mathbf{u}}{dt} - \mathbf{g}\right) \cdot \mathbf{v} dx - \int_\Omega p \nabla . \mathbf{v} \, dx + \int_\Omega 2\eta_s \mathbf{D}[\mathbf{u}] : \mathbf{D}[\mathbf{v}] dx - \int_\Omega \mathbf{v} . \nabla . \left(\frac{c}{\lambda_r} \mathbf{A}\right) dx$$
$$- \int_\Omega \gamma \kappa \delta(\phi) \mathbf{n} \cdot \mathbf{v} \, dx = 0$$

$$\text{for all } \mathbf{v} \in W_{u0}, \tag{6.7}$$

$$\int_\Omega q \nabla . \mathbf{u} \, dx = 0 \quad \text{for all } q \in L^2(\Omega), \tag{6.8}$$

$$\mathbf{u}|_{t=0} = \mathbf{u}_o \quad \text{in } \Omega, \tag{6.9}$$

$$\int_\Omega \left(\frac{\partial \mathbf{A}}{\partial t} + \mathbf{u} \cdot \nabla \mathbf{A} - \mathbf{A} \cdot \nabla \mathbf{u} - \nabla \mathbf{u}^T \cdot \mathbf{A} + \frac{1}{\lambda_r}(\mathbf{A} - \mathbf{I})\right) \cdot \mathbf{s} \, dx = 0 \qquad \text{for all } \mathbf{s} \in W_{A0}, \tag{6.10}$$

$$\mathbf{A}|_{t=0} = \mathbf{A}_o \quad \text{in } \Omega, \tag{6.11}$$

$$\int_\Omega \left(\frac{\partial \phi}{\partial t} + \mathbf{u} \cdot \nabla \phi \right) g \, d\mathbf{x} = 0 \text{ for all } g \in W_{\phi 0}, \tag{6.12}$$

$$\phi|_{t=0} = \phi_0 \quad \text{in } \Omega.$$

6.5 Finite-Element Approximation

In order to solve the above problem numerically, one will discretize the domain using a regular finite element triangulation T_h for the velocity and configuration tensor, where h is the mesh size, and a regular triangulation T_{2h} for the pressure. The following finite dimensional spaces are defined for approximating W_u, W_{u0}, W_A, W_{A0}, $L^2(\Omega)$, $L^2_0(\Omega)$, W_ϕ and $W_{\phi 0}$:

$$W_{u,h} = \{\mathbf{v}_h \in C^0(\overline{\Omega})^2 \mid \mathbf{v}_h|_T \in P_1 \times P_1 \text{ for all } T \in T_h, \mathbf{v}_h = \mathbf{u}_{\Gamma,h} \text{ on } \Gamma\}$$

$$W_{0,h} = \{\mathbf{v}_h \in C^0(\overline{\Omega})^2 \mid \mathbf{v}_h|_T \in P_1 \times P_1 \text{ for all } T \in T_h, \mathbf{v}_h = 0 \text{ on } \Gamma\} \tag{6.13}$$

$$L^2_h = \{q_h \in C^0(\overline{\Omega}) \mid q_h|_T \in P_1 \text{ for all } T \in T_{2h}\}$$

$$L^2_{0,h} = \{q_h \in L^2_h \mid \int_\Omega q_h \, d\mathbf{x} = 0\} \tag{6.14}$$

$$W_{A,h} = \{\mathbf{s}_h \in C^0(\overline{\Omega})^3 \mid \mathbf{s}_h|_T \in P_1 \times P_1 \times P_1 \text{ for all } T \in T_h, \mathbf{s}_h = \mathbf{A}_{L,h} \text{ on } \Gamma^-\}$$

$$W_{A0,h} = \{\mathbf{s}_h \in C^0(\overline{\Omega})^3 \mid \mathbf{s}_h|_T \in P_1 \times P_1 \times P_1 \text{ for all } T \in T_h, \mathbf{s}_h = 0 \text{ on } \Gamma^-\} \tag{6.15}$$

$$W_{\phi,h} = \{g_h \in C^0(\overline{\Omega}) \mid g_h|_T \in P_1 \text{ for all } T \in T_h, g_h = \phi_{0,h} \text{ on } \Gamma^-\}$$

$$W_{\phi 0,h} = \{g_h \in C^0(\overline{\Omega}) \mid g_h|_T \in P_1 \text{ for all } T \in T_h, g_h = 0 \text{ on } \Gamma^-\} \tag{6.16}$$

$$W_{\phi R,h} = \{g_h \in C^0(\overline{\Omega}) \mid g_h|_T \in P_1 \text{ for all } T \in T_h, g_h = 0 \text{ on the interface}\}. \tag{6.17}$$

Using these finite dimensional spaces, the following finite-element approximation to the problem (6.7) -(6.13), the following is obtained:

Find $\mathbf{u}_h \in W_{u,h}$, $\mathbf{A}_h \in W_{A,h}$, $\phi_h \in W_{\phi,h}$ and $p_h \in L^2_{0,h}$, satisfying

$$\int_\Omega \rho_L \left(\frac{d\mathbf{u}_h}{dt} - \mathbf{g} \right) . \mathbf{v}_h \, d\mathbf{x} - \int_\Omega p_h \nabla . \mathbf{v}_h \, d\mathbf{x} + \int_\Omega 2\eta_s \mathbf{D}[\mathbf{u}_h] : \mathbf{D}[\mathbf{v}_h] d\mathbf{x} - \int_\Omega \mathbf{v}_h . \nabla . \left(\frac{c}{\lambda_r} \mathbf{A}_h \right) d\mathbf{x}$$
$$- \int_\Omega \gamma \kappa \delta(\phi) \mathbf{n} \cdot \mathbf{v} \, d\mathbf{x} = 0$$

for all $\mathbf{v}_h \in W_{0,h}$,

$$\int_\Omega q_h \nabla . \mathbf{u}_h \, d\mathbf{x} = 0 \qquad \text{for all } q_h \in L^2_h,$$

$$\int_\Omega \left(\frac{\partial \mathbf{A}_h}{\partial t} + \mathbf{u}_h . \nabla \mathbf{A}_h - \mathbf{A}_h . \nabla \mathbf{u}_h - \nabla \mathbf{u}_h^T . \mathbf{A}_h + \frac{1}{\lambda_r} (\mathbf{A}_h - \mathbf{I}) \right) . \mathbf{s}_h \, d\mathbf{x} = 0$$

for all $\mathbf{s}_h \in W_{A0,h}$,

$$\int_\Omega \left(\frac{\partial \phi_h}{\partial t} + \mathbf{u}_h . \nabla \phi_h \right) g_h \, d\mathbf{x} = 0$$

for all $g_h \in W_{\phi 0,h}$,

$$\mathbf{u}|_{t=0} = \mathbf{u}_{0,h} \qquad \text{in } \Omega,$$

$$\mathbf{A}_h|_{t=0} = \mathbf{A}_{0,h} \qquad \text{in } \Omega,$$

$$\phi|_{t=0} = \phi_{0,h} \qquad \text{in } \Omega. \qquad (6.18)$$

6.6 Time Discretization

The initial value problem is solved by using the Marchuk-Yanenko operator splitting scheme (Singh 1993) which allows to decouple its four primary difficulties:

1. The incompressibility condition, and the related unknown pressure p_h,
2. The nonlinear advection term,
3. The interface problem, and the related unknown level set distribution ϕ_h
4. The equation for the configuration tensor, and the viscoelastic stress tensor which appears in the momentum equation.

The Marchuk-Yanenko operator splitting scheme can be applied to an initial value problem of the form

$$\frac{d\phi}{dt} + A_1(\phi) + A_2(\phi) + A_3(\phi) + A_4(\phi) = f$$

where the operators A_1, A_2, A_3, and A_4 can be multiple-valued. Let Δt be the time step, and α, β and γ be three constants: $0 \leq \alpha, \beta, \gamma \leq 1$ and $\alpha + \beta + \gamma = 1$. Use the following version of the Marchuk-Yanenko operator splitting to simulate the motion of particles in a viscoelastic fluid:

Set $\mathbf{u}^0 = \mathbf{u}_{0,h}$, $\mathbf{A}^0 = \mathbf{A}_{0,h}$, and $\phi^0 = \phi_{0,h}$.

For n=0,1,2,... assuming $\mathbf{u}^n$, $\mathbf{A}^n$, and ϕ^n are known, find the values for n+1 using the following:

STEP 1:

Find $\mathbf{u}^{n+1/4} \in W_{u,h}$ and $p^{n+1/4} \in L^2_{0,h}$, by solving

$$\int_\Omega \rho \frac{\mathbf{u}^{n+1/4}-\mathbf{u}^{n}}{\Delta t}.\mathbf{v}\,d\mathbf{x} - \int_\Omega p^{n+1/4}\nabla.\mathbf{v}\,d\mathbf{x} + \alpha\int_\Omega 2\eta_s \mathbf{D}[\mathbf{u}^{n+1/4}]:\mathbf{D}[\mathbf{v}]d\mathbf{x}$$
$$= \int_\Omega \mathbf{v}.\nabla.\left(\frac{c}{\lambda_s}\mathbf{A}^{n}\right)d\mathbf{x} + \int_\Omega \gamma\kappa\delta(\phi)\mathbf{n}\cdot\mathbf{v}\,d\mathbf{x} + \int_\Omega \rho_L \mathbf{g}\,\mathbf{v}d\mathbf{x}$$

for all $\mathbf{v} \in W_{0,h}$,

$$\int_\Omega q\nabla.\mathbf{u}^{n+1/4}\,d\mathbf{x} = 0 \qquad \text{for all } q \in L^2_h, \tag{6.19}$$

STEP 2:

Find $\mathbf{u}^{n+2/4} \in W_{u,h}$, by solving

$$\int_\Omega \rho \frac{\mathbf{u}^{n+2/4}-\mathbf{u}^{n+1/4}}{\Delta t}.\mathbf{v}d\mathbf{x} + \int_\Omega \rho_L(\mathbf{u}^{n+2/4}.\nabla\mathbf{u}^{n+2/4}).\mathbf{v}\,d\mathbf{x} + \beta\int_\Omega 2\eta_s\mathbf{D}[\mathbf{u}^{n+2/4}]:\mathbf{D}[\mathbf{v}]d\mathbf{x} = 0$$

for all $\mathbf{v} \in W_{0,h}$, (6.20)

STEP 3:

Find $\mathbf{A}^{n+3/4} \in W_{A,h}$, by solving

$$\int_\Omega \left(\frac{\mathbf{A}^{n+3/4}-\mathbf{A}^{n}}{\Delta t} + \mathbf{u}^{n+2/4}.\nabla\mathbf{A}^{n+3/4} - \mathbf{A}^{n+3/4}.\nabla\mathbf{u}^{n+2/4} - (\nabla\mathbf{u}^{n+2/4})^{T}.\mathbf{A}^{n+3/4} + \frac{1}{\lambda_r}(\mathbf{A}^{n+3/4}-\mathbf{I})\right).\mathbf{s}\,d\mathbf{x}$$
$=0$

for all $\mathbf{s} \in W_{A0,h}$, (6.21)

STEP 4:

Find $\phi^{n+4/4} \in W_{\phi,h}$, by solving

$$\int_\Omega \left(\frac{\phi^{n+4/4} - \phi^n}{\Delta t} + \mathbf{u}^{n+2/4} . \nabla \phi^{n+4/4} \right) g_h \, d\mathbf{x} = 0$$

for all $g_h \in W_{\phi 0,h}$. (6.22)

Set $\mathbf{u}^{n+1} = \mathbf{u}^{n+2/4}$, $\mathbf{A}^{n+1} = \mathbf{A}^{n+3/4}$, $p^{n+1} = p^{n+1/4}$, $\phi^{n+1} = \phi^{n+4/4}$.

STEP 5:

Reinitialize ϕ^{n+1}

Set $\phi_R^0 = \phi^{n+1}$

For r = 0, 1, 2, ...

$$\mathbf{w}^r = S(\phi^{n+1}) \frac{\nabla \phi_R^r}{|\nabla \phi_R^r|}$$

Find $\phi_R^{r+1} \in W_{\phi R,h}$, by solving

$$\int_\Omega \left(\frac{\phi_R^{r+1} - \phi_R^r}{\Delta t} + \mathbf{w}^r . \nabla \phi_R^r \right) g_h \, d\mathbf{x} = \int_\Omega S(\phi^{n+1}) \, g_h \, d\mathbf{x}$$

for all $g_h \in W_{\phi R,h}$. (6.23)

go back to the above for loop.

Set $\phi^{n+1} = \phi_R^{r+1}$ and go back to the first step.

Remarks:

1. The first step gives rise to a Stokes-like problem for the velocity and pressure distributions which is solved by using a conjugate gradient method Sussman (1994).

2. The second step is a nonlinear problem for the velocity, which is solved by using a least square conjugate gradient algorithm (Pillapakkam 2001).

3. The third step is a linearized hyperbolic problem for the configuration tensor or stress. This problem is solved by using a third order upwinded positive only scheme (Glowinski 1998). The two key features of this scheme are: a positive only scheme that guarantees the positive definiteness of the configuration tensor, and a third order upwinding scheme for discretizing the convection term in the constitutive equation. These two features are important for obtaining a scheme that is stable at relatively large Deborah numbers.

4. The fourth step is a hyperbolic problem for the scalar level set function ϕ. This problem is solved by using a upwinding scheme where the convection term is discretized using a third order scheme (Glowinski 1998). After advecting ϕ, reinitialize ϕ to be a distance function near the interface by performing two iterations of (6.23).

CHAPTER 7

RESULTS

The direct simulation results for the motion of leukocytes in pressure driven flows in three dimensional channels with rectangular cross sections are described in this chapter. Letting the pressure gradient in the channel be $\frac{dp}{dz}$, the velocity profile of a Newtonian fluid in a two dimensional channel is $w(x) = \frac{1}{2\mu}\frac{dp}{dz}x(x-h)$, with a corresponding shear stress equal to $\frac{1}{2\mu}\frac{dp}{dz}(2x-h)$. Notice that the shear stress varies linearly with x, that its maximum value is at the channel wall and that it is zero at the channel center. In simple shear flows, the stretching occurs along the direction which makes an angle of 45° with the flow direction, and the stretched material elements rotate due to the flow vorticity which is aligned with the negative y-axis.

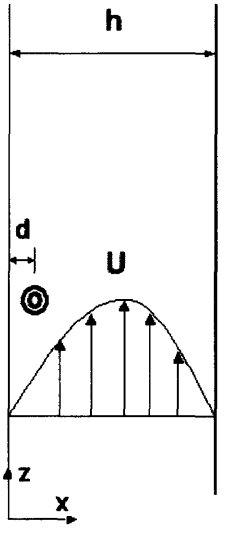

Figure 7.1 Leukocyte in a pressure driven flow – model set up.

Firstly, consider the case where the adhesive force between the wall and the leukocytes is not present, and thus the behavior of a leukocyte is similar to that of a drop in a pressure driven flow. In a pressure driven flow, since the shear stress is maximum at the channel wall and decreases linearly with increasing distance from the channel wall, the deformation is expected to be maximum when the leukocyte is close to the wall and to decrease with increasing distance from the wall.

Besides the study on the cell's deformation, the lateral motion of the cell in the pressure driven flow are presented below as well using the two composite drop models – composite-drop model and drop-rigid particle model. An equilibrium location for white blood cell in blood flow is found.

Secondly, consider the motion of a leukocyte released near the channel wall at a distance such that the adhesion force is present. The objective here is to study its motion and deformation under the combined action of the adhesive and hydrodynamic forces. Both models of the adhesive force, i.e., the potential model and the kinetic model as described in Chapter 3 are investigated.

Thirdly, to investigate the influence of the capillary walls unevenness on the motion and deformation of the leukocyte the unevenness, a layer periodically arranged rigid spheres is used to cover the lower surface of the channel.

For most cases reported, the dimensionless parameters are Re=0.5, Ca=0.167, De= 0.1 and Adh=50.0. For some cases Re, Ca and Adh are varied.

Finally, these simulation results are compared with the laboratory observations of the rolling and deformation of leukocyte through parallel plate chamber.

7.1 Leukocyte Deformation in the Absence of Adhesion Force

7.1.1 Composite-Drop Model

Figure 7.2 shows the steady state leukocyte shapes for the compound drop model at various distances from the channel wall. In all cases, both the outer layer and the nucleus of the leukocyte are deformed. In addition, as noted above, the deformation of the leukocyte is greater when it is closer to the channel wall. As far as its orientation is concerned, the angle between the principal axis of the deformed shape and the channel wall is smaller when it is closer to the wall. Also interesting is the fact that the angle between the principal axis of the deformed nucleus and the wall is greater than that between the deformed cell and the wall. Notice that both the leukocyte and the nucleus are deformed. The deformation increases with decreasing gap between the leukocyte and the wall. Moreover, the viscoelastic stresses inside the nucleus are maximal in the region which is closest to the wall as shown in Figure 7.3. The Reynolds number is 0.5.

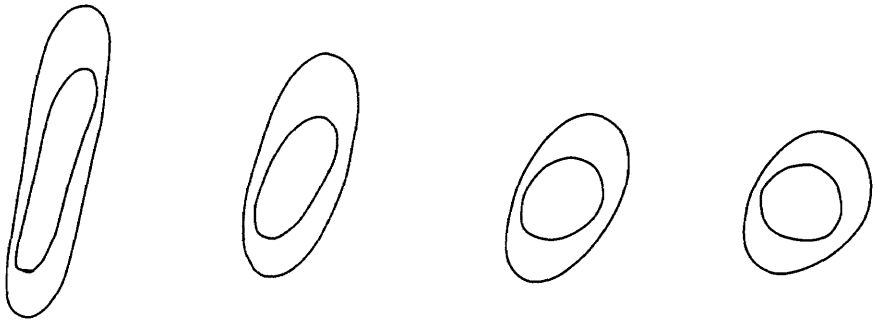

Figure 7.2. Leukocyte deformation in the case of the compound-drop model at different distances from the wall. The shape on the xz-mid plane through the leukocyte center are shown. (a) x=1.9, (b) x=2.425, (c) x=2.9, and (d) x=3.375 at time t=4.6. The deformation increases with decreasing gap between the leukocyte and the wall. Notice that both the leukocyte and the nucleus are deformed. The Reynolds number is 0.5.

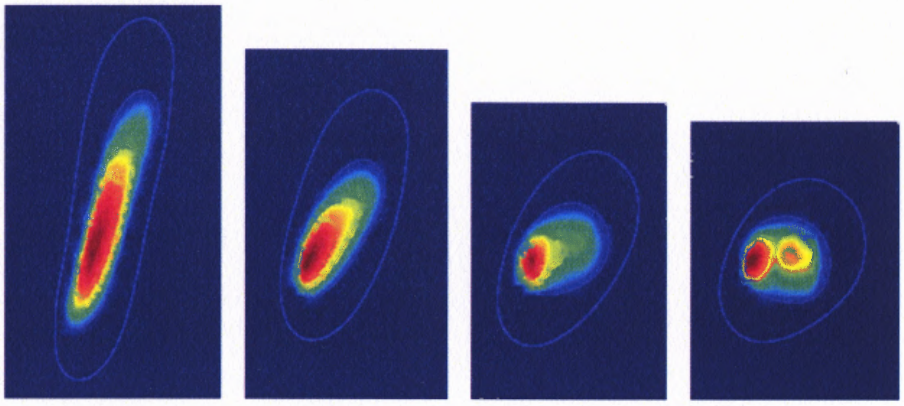

(a) (b) (c) (d)

Figure 7.3 Viscoelastic stresses contour on the xz-mid plane through the leukocyte center in the case of the compound-drop model at different distances from the wall is shown at (a) x=1.9, (b) x=2.425, (c) x=2.9, and (d) x=3.375 at time t=4.6. The Reynolds number is 0.5.

7.1.2 Drop-Rigid Particle Model

In the drop-rigid-particle model, since the nucleus is modeled as a rigid sphere, it remains spherical while the outer layer of the leukocyte deforms. The steady deformed shapes for the drop-rigid-particle model at various distances from the wall are shown in Figure 7.4. The remaining parameters are the same as in Figure 7.2. From Figures 7.3 and 7.4, it is clear that the overall deformation is smaller for the drop-rigid-particle model which is a consequence of the fact that the nucleus does not deform. This implies that the drop-rigid-particle model is not appropriate for situations in which the cell, as well as the nucleus, deform significantly, such as during spreading or transmigration. Figure 7.5 shows the steady shape of a leukocyte released at a distance of x=2 from the wall. It is stretched and its principal direction makes an angle of ~40 degrees with the channel wall. The simulations show that the leukocyte is moving laterally, away from the channel wall, while moving in the flow direction. This is also the case for the compound-drop model

described in the previous subsection. The lateral migration of single freely suspended leukocyte cell in blood flows will be discussed in the next subsection.

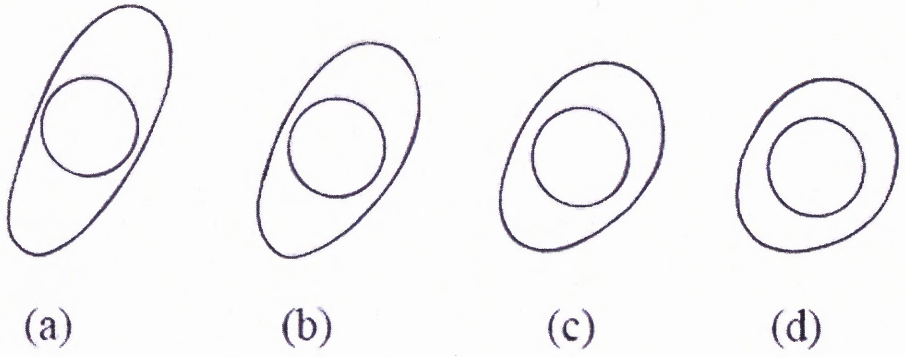

Figure 7.4 Leukocyte deformations in the case of the drop-rigid-particle model as a function of the distance from the wall. (a) x=1.9, (b) x=2.425, (c) x=2.9, and (d) x=3.375 at time t=4.6. The deformation increases with decreasing gap between the leukocyte and the wall. Since the nucleus is rigid, it does not deform. The Reynolds number is 0.5.

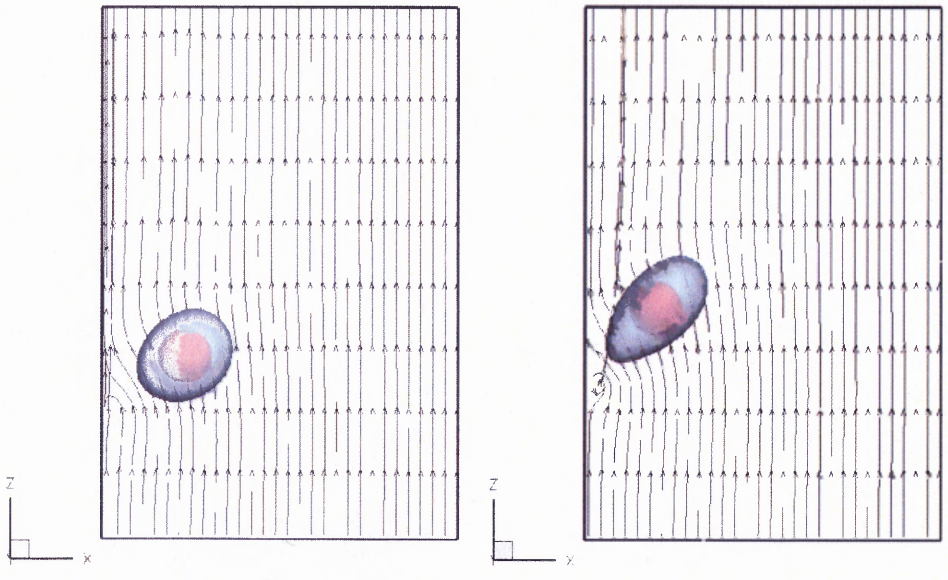

Figure 7.5 Deformation of a leukocyte represented by the drop-rigid-particle model at (a) t=0.82 and (b) t=5.25. The Reynolds number is 0.5.

7.2 Lateral Migrations of Leukocyte in the Absence of Adhesion Force

Past studies of the motion of drops in the pressure driven flows, as discussed in Section 2.3, have shown that a drop not only moves in the flow direction, but also drifts laterally. The velocity of the lateral drift, however, is very small compared to the velocity in the flow direction. Therefore, regardless of the initial position of the drop, it eventually, after a relatively large displacement in the flow direction, reaches a lateral equilibrium position, which depends on the ratio of the viscosity of the fluid inside the drop and that of the surrounding fluid.

For the parameter values considered in this study, the Reynolds number is 0.5, and the ratio of the cytoplasm and plasma viscosities is 100. The lateral migration of leukocytes, released at different distances from the wall of the channel, is studied in a periodic domain. The initial positions ranged between x= 1.475 and x=3.375. The channel wall is at x=0 and the centerline of the channel is at x=3.85.

Some of the numerically obtained trajectories of leukocytes' centers of mass are displayed in Figure 7.6. The depicted simulations show that the lateral equilibrium position of a leukocyte is around x=2.5, which is approximately at a distance of 0.32 h from the channel wall, where h is the channel height. This implies that a leukocyte cannot be captured at a wall unless it is brought closer to the wall by some other mechanism, e.g., by collisions with other blood cells. This result is also relevant to the experimental studies directed at investigating the adhesion mechanisms between the endothelial monolayer and an isolated leukocyte, i.e., when no other blood cells are present. The illustrated results indicate that once the flow is started, a leukocyte is likely to stay away from the wall, unless it is placed near the wall at the beginning.

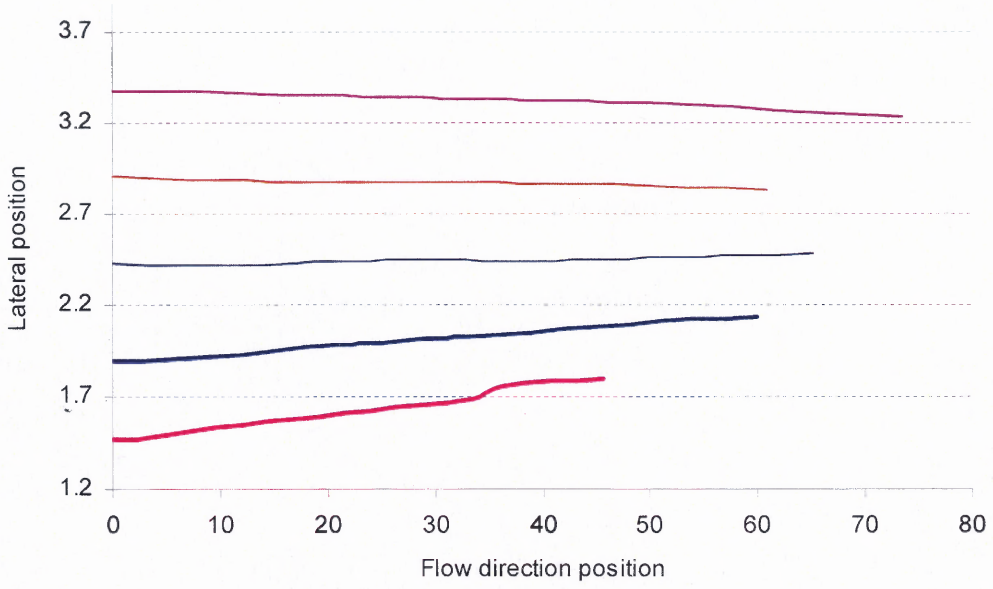

Figure 7.6 Trajectories of leukocytes released from different positions within the channel. The Reynolds number is 0.5.

This lateral equilibrium location for leukocytes in the blood flows is quite far from the channel wall, and it shows that leukocytes cannot to be captured and strongly adhered to the wall automatically without additional adhesive force.

7.3 Under Adhesive Force on the Channel Wall

In this section, the motion of a leukocyte released near the channel wall at a distance such that the adhesion force is present is studied. The objective is to study its motion and deformation under the combined action of the adhesive and hydrodynamic forces. Both models of the adhesive force, i.e., the potential model and the kinetic model as described in Chapter 4 are considered.

In the presence of a pressure driven flow, the leukocyte experiences a hydrodynamic lift force whose magnitude depends on many factors including the flow velocity. If the lift force is larger than the adhesion force, the leukocyte moves away from

the wall. Obviously, when the flow velocity is smaller than a critical value such that the lift force is smaller than the adhesive force, the leukocyte is expected to remain attached to the wall. The case where the bulk pressure driven flow is not present is the limiting case for which the hydrodynamic lift force is zero. This case is considered first. Then the flow is applied on driven by a pressure gradient. By varying and studying the role of the dimensionless parameters such as Reynolds number (Re), Capillary number (Ca), Adhesion number (Adh), the critical condition under which the leukocyte cell can remain attached can be understood.

7.3.1 Absence of pressure driven flow

In the absence of a bulk pressure driven flow, the only forces acting on the leukocyte is the adhesive force which moves and deforms it and hydrodynamic force due to this motion/deformation so that the total force acting on the leukocyte becomes zero. Figure 7.7 shows that the leukocyte's surface deforms and becomes flat near the wall. The surface tension, however, resists this flattening of the interface and a deformed steady shape is reached for which the deforming adhesive force is balanced by the surface tension force. Notice that the flattening is relatively smaller for the kinetic adhesion model which is a consequence of the fact that the distance range over which the force acts is much smaller.

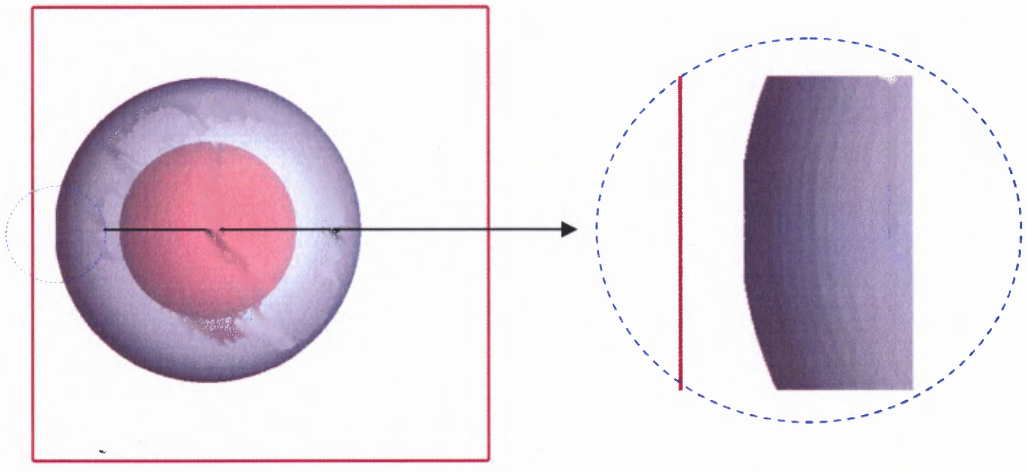

(a)

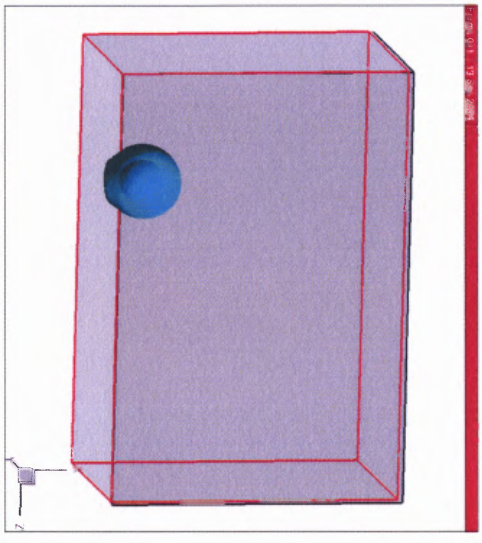

(b)

Figure 7.7 Deformation of a leukocyte near the wall due to the adhesion force in the absence of a pressure driven flow. The adhesion parameter is 50.0. Notice that the surface near the wall, as shown in the magnified view, is flat. (a) Kinetic model, t=0.6 s, (b) potential model, t=0.6.

7.3.2 Adhesion Potential Model: Motion near a Smooth Wall

In a pressure driven flow, in addition to the adhesion force the leukocyte also experiences a hydrodynamic force. The component of the hydrodynamic force in the flow direction, or drag, moves it in the flow direction; and the component normal to the wall, or lift,

moves it away from the wall, thus countering the adhesion force acting towards the wall. In this subsection, the case where the adhesive force is given by the potential model and the wall is smooth is considered. The adhesion potential strength and the initial leukocyte position of x=2.0 were selected so that the leukocyte is attracted to the wall. First consider the case of the drop-rigid-particle model.

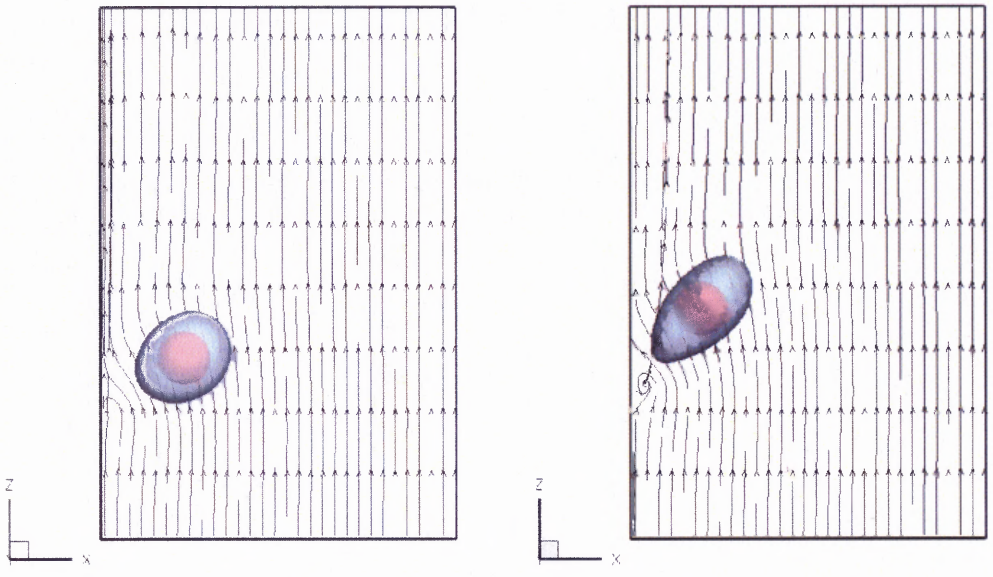

(a) (b)

Figure 7.8 Deformation of a leukocyte in the case of the drop-rigid-particle model due to shear forces while it moves towards the wall under the action of the adhesive force at (a) t=0.82 and (b) t=2.46. The Reynolds number is 0.5, Ca=0.167, De= 0.1 and Adh=50.0.

The flow causes the leukocyte to stretch along the shear direction, while the adhesive force pulls it towards the wall (see Figure 7.8). The adhesive force in the potential model is long-ranged, which can be seen by the fact that a leukocyte located at a short distance from the wall is pulled towards the wall. This feature of the potential model is perhaps unrealistic since the adhesive forces are not long-ranged. Remind that the force for the kinetic model is very short-ranged (as discussed in Section 4.2.2). The adhesion force is present only over the narrow distance range of 30 nm. As the trailing

end of the deformed leukocyte is closer to the wall, it experiences a larger attractive potential force, and thus is pulled further towards the wall. Consequently, the trailing end of the leukocyte begins to flatten, and the contact area between the leukocyte and the wall begins to increase. The contact area continues to increase until the surface tension force becomes equal to the deforming forces. When similar simulations are performed using the compound-drop model, the nucleus of the leukocyte also deforms as shown in Figure 7.10. The other features of the overall deformation are similar. Here, the initial position of the center of the leukocyte is x=0.5. The flow causes the leukocyte to move upwards, and the adhesive and shear forces cause the surface of the leukocyte near the wall to flatten. Furthermore, it is interesting to note that the gap between the leukocyte surface and the wall near the leading edge is larger than that near the trailing edge. Notice that this flattening of the leukocyte cannot be seen in the top view where it appears to be only elongated (Chaotard-Ghodsnia 2002). This is an important point because in experiments only the top view can be accessed generally.

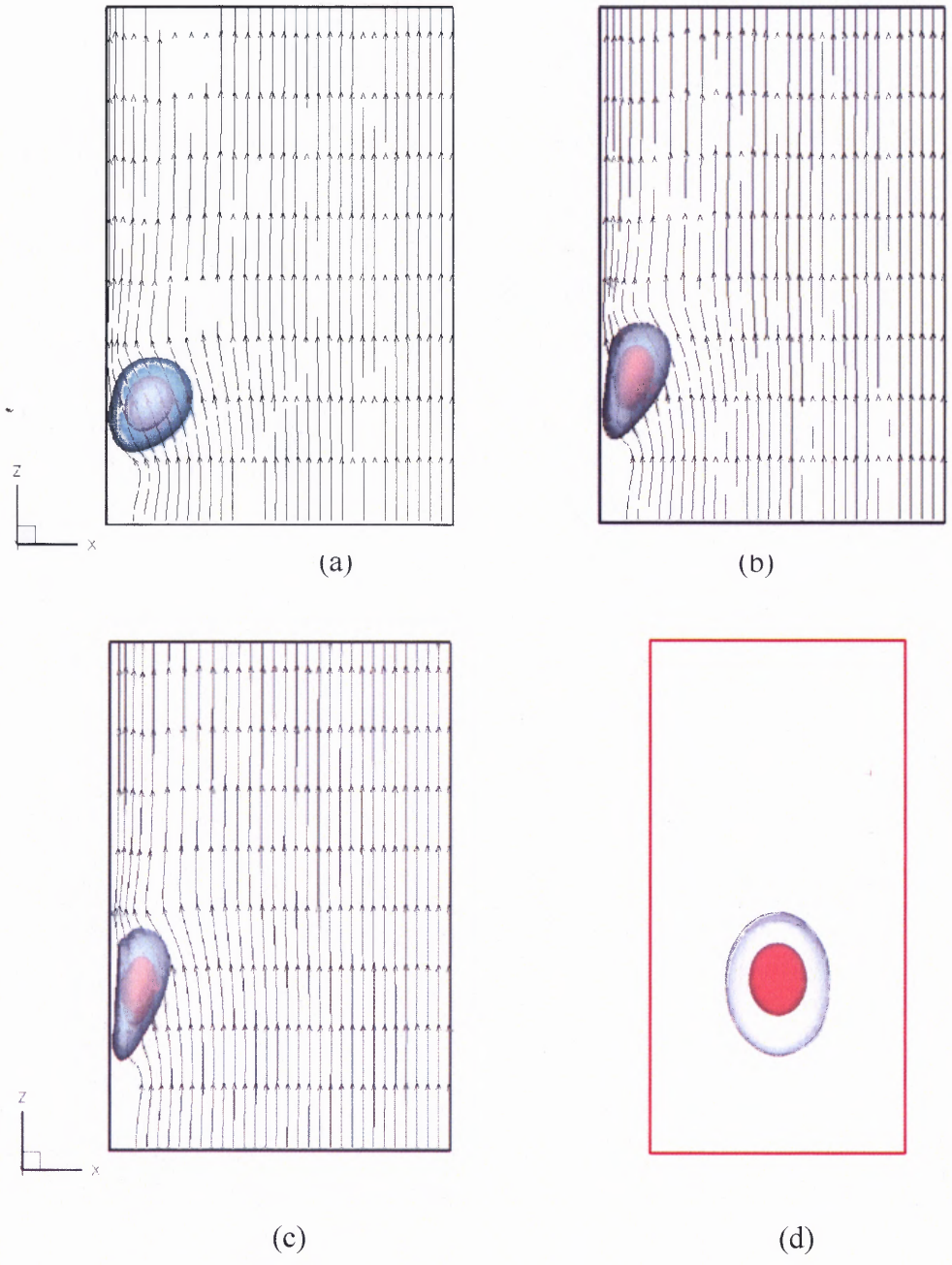

Figure 7.9 Leukocyte deformation in the case of the compound-drop model released close to the wall at (a) t=0.82, and (b) t=2.46, and (c) t=3.94. The top view is also shown (d). The Reynolds number is 0.5, Ca=0.167, De= 0.1 and Adh=50.0.

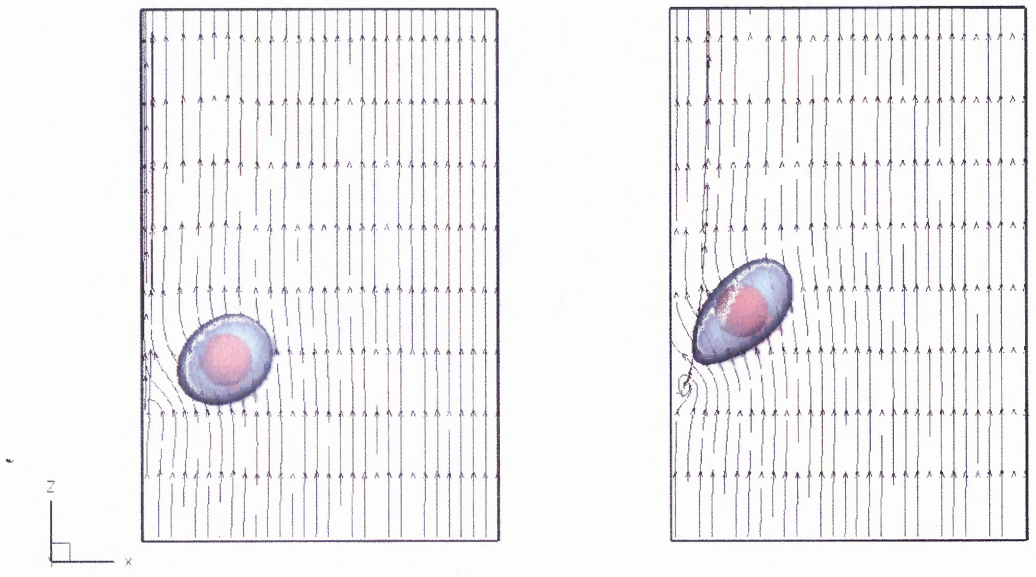

(a) (b)

Figure 7.10 Deformation of a leukocyte represented by the drop-rigid-particle model due to the shear forces while it moves towards the wall under the action of the adhesive force at (a) t=0.82 and (b) t=2.46.

7.3.3 Adhesion Potential model: Motion near a Wall Covered with Rigid Spheres

To investigate the influence of the capillary walls unevenness on the motion and deformation of the leukocyte, consider the case where the lower surface of the channel consists of a flat wall covered by a layer of rigid spheres as shown in Figure 7.11 (a). The fluid velocity in the region occupied by the particles is enforced to be zero by using the distributed Lagrange multiplier method. These spheres mimic the endothelial cells that cover the inner layer of blood vessels. The distance x in the adhesion model is measured from the x=1.1 plane which is tangential to the spheres and thus the leukocyte is attracted to this plane.

The spheres are assumed to be fixed at their locations and thus the fluid velocity on their surfaces is zero. The fluid velocity in the x=1.1 plane which is tangential to the spheres is, however, uneven; it is zero at the points where the spheres touch the plane and

largest in the middle of the gaps between the spheres. The shear rate and vorticity also vary on the x=1.1 plane. Figure 7.11 (b) shows that the volume averaged velocity of the leukocyte varies as it moves in the flow direction (see Figure 7.11b). It appears to slip when its lower surface is in between the gap between the spheres and stick, or slow down, when the lower surface comes close to the spheres' surfaces. The initial velocities of the points inside and on the leukocyte boundary were assumed to be the same as for the pressure driven flow, and thus the velocity initially decreases because the leukocyte deforms and its lower surface becomes flattened. The velocity of a leukocyte moving near a smooth wall, on the other hand, is approximately constant.

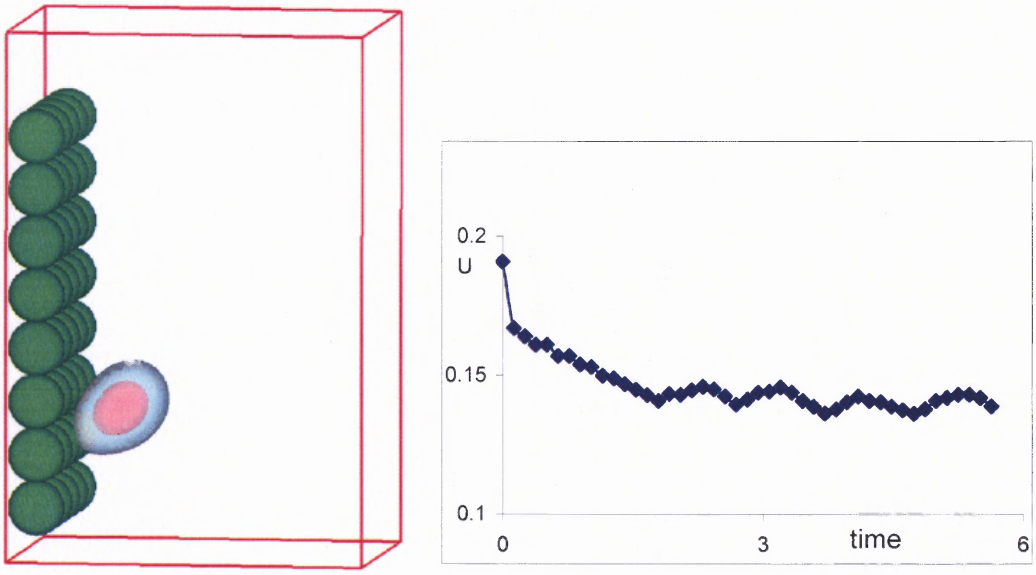

(a) (b)

Figure 7.11 Motion of a leukocyte near an uneven wall consisting of a layer of spheres. (a) The spheres are arranged on a rectangular lattice and initially the lower surface of the leukocyte is tangential to the x=1.1 plane. (b) Leukocyte dimensionless velocity as a function of time for Re=0.5, Ca=0.084, De= 0.1 and Adh=50.0.

Figure 7.12 shows that the leukocyte stretches along the shear direction and is pulled towards the x=1.1 plane by the adhesive force. The trailing end of the deformed leukocyte, which is closer to the x=1.1 plane, which experiences a larger attractive adhesive force, is pulled towards the layer of spheres and flattens. The contact area continues to increase while the leukocyte moves downstream. Also notice that, as in Figure 7.10, the gap between the leukocyte surface and the wall is larger near the leading edge than near the trailing edge. The deformed shape of the leukocyte in Figure 7.12 is, however, qualitatively different from that in Figure 7.10. Specifically, in Figure 7.12, the flattened area over which the adhesive force acts is relatively smaller and the angle the major axis of the deformed leukocyte makes with the plane tangent to the spheres is greater. The latter is also true for the deformed nucleus. In the top view it appears elongated in the flow direction with the trailing end being more pointed than the leading edge. In Figure 7.13 the motion of a leukocyte is shown for Ca=0.084 with all other parameters being the same as in Figure 7.12 (where Ca=0.167). Since the capillary number is smaller, the deformation is smaller. Also notice that in this case the shape of the leukocyte becomes steady, and is approximately the same in Figures 7.13b and c. The lateral velocity of the leukocyte varies as it rolls over the layer of spheres. Again, notice that the deformed shape of the leukocyte qualitatively differs from that in Figure 7.10. These differences in the shapes are a result of the fact that the fluid velocity on the plane tangent to the spheres is not identically zero, whereas the fluid velocity on a flat wall is zero. Also notice that the shape of the leukocyte is qualitatively similar to that in Figure 7.22 for experiments where the leukocyte is elongated and the radius near the leading edge is larger than near the trailing edge.

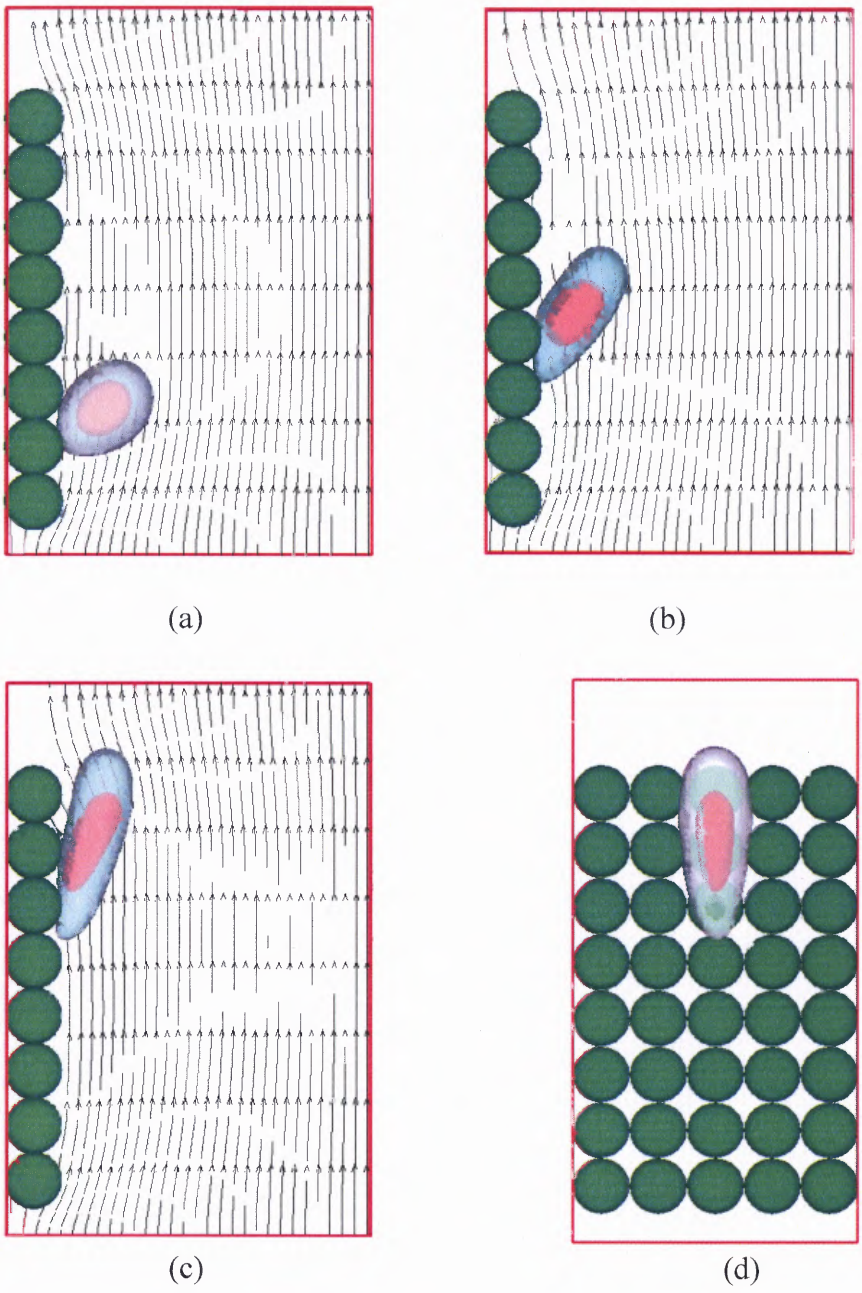

Figure 7.12 Leukocyte deformation in the case of the compound-drop model released close to an uneven wall consisting of a layer of rigid spheres. The parameters are Re=0.5, Ca=0.167, De= 0.1 and Adh=50.0. (a) t=0.82, (b) t=2.46, and (c) t=4.92. Both side and top views are shown.

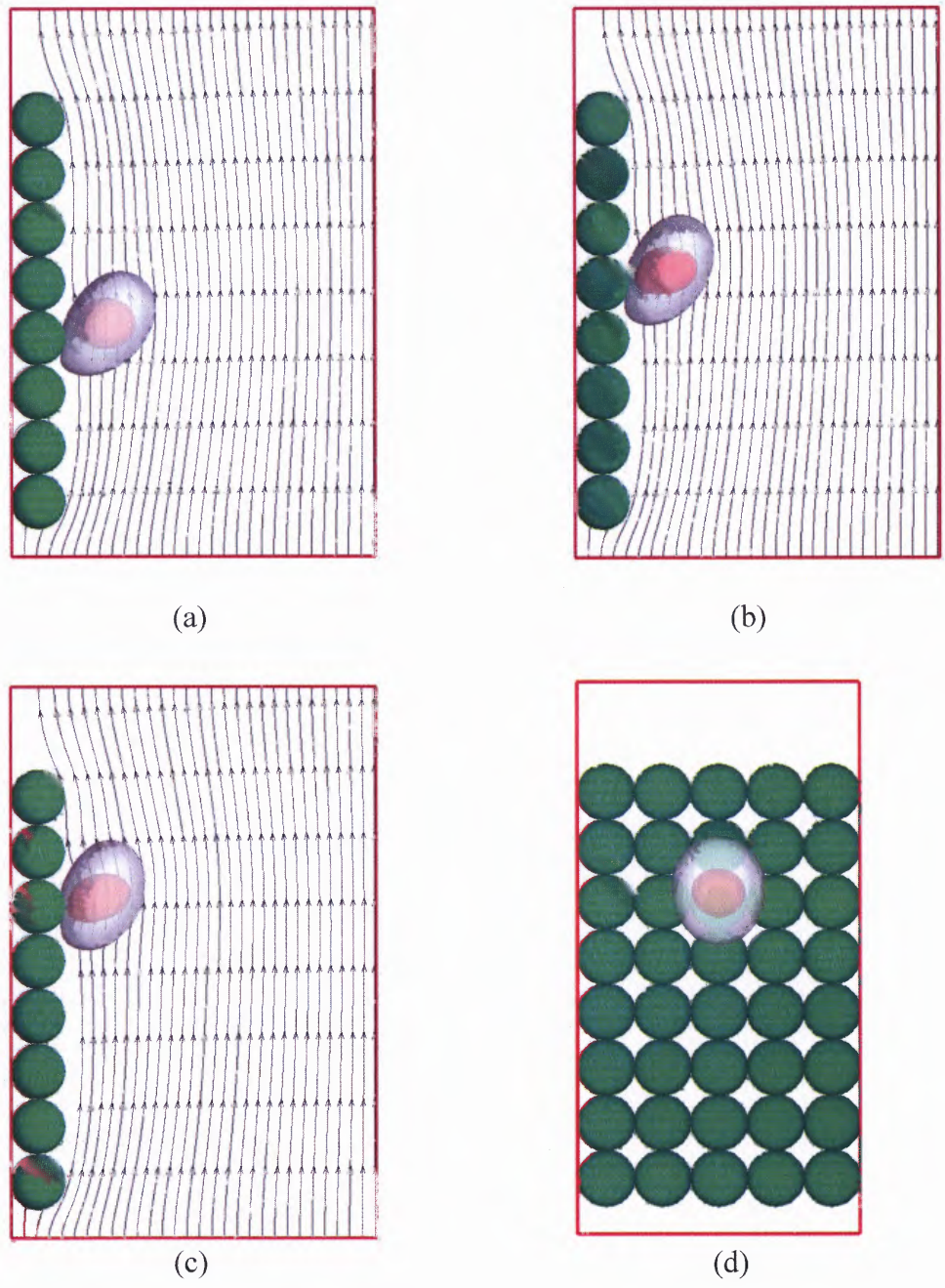

Figure 7.13 Leukocyte deformationin the case of the compound-drop model released close to an uneven wall formed with a layer of rigid spheres. The parameters are the same as in Figure 7.12, except for the capillary number which is now Ca=0.084.

7.3.4 Kinetic Adhesion Model: Pressure Driven Flow

As noted above, the adhesion force for the kinetic model is non-zero for a very small range of distances between the leukocyte surface and the wall. Therefore, for the results presented in this section the initial position of the leukocyte is selected in a manner that the force is present. Figure 7.14 shows that at the beginning the leukocyte rolls near the wall surface. The Reynolds number for this case is 0.5. As the leukocyte deforms, the lift force it experiences increases and in this case the leukocyte moves away from the wall as the adhesion force is not sufficiently large to keep it attached. This is in agreement with Cantat and Misbah (1999) and Khismatullin and Truskey (2004). After the leukocyte moves out of the range of the kinetic adhesion force, which as noted above corresponds to the relatively short distance of about 30 nm, the adhesion force becomes zero. The leukocyte then migrates to a lateral distance at which the lateral hydrodynamic force is zero, as discussed in Section 4.2.2.

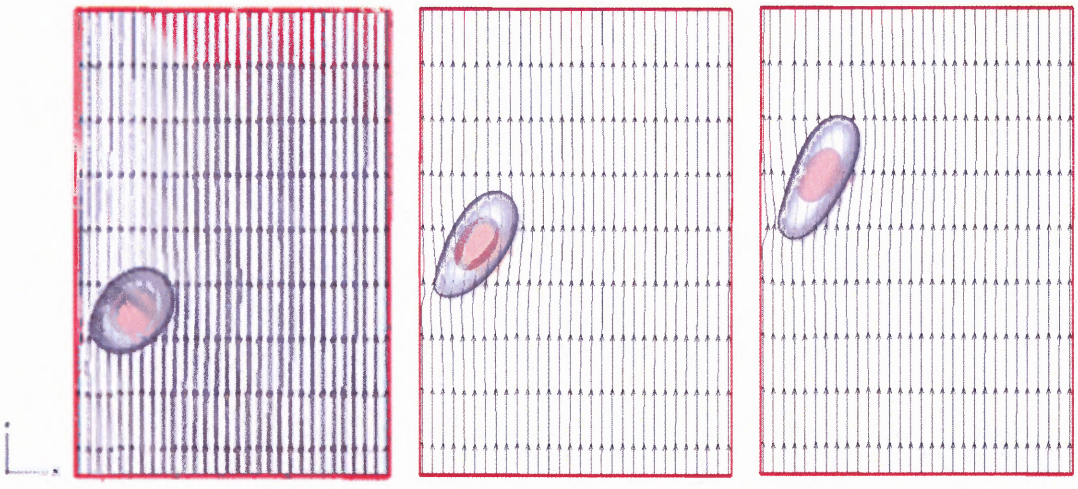

(a) (b) (c)

Figure 7.14 Leukocyte deformation in the case of the compound-drop model and the adhesion force given by the kinetic model at (a) t=0.6, (b) t=3, and (c) t=6, for a Reynolds number of Re=0.5, Ca=0.167, De= 0.1 and Adh=50.0.

Next consider the case where the adhesion force is 100 times larger and the adhesion parameter is 5000. The adhesion force was increased by this rather large factor to ensure that the leukocyte is captured at the wall. In this case, the cell remained attached to the wall, as shown in Figure 7.15. After the steady state is reached and the deformation no longer increases, the lower area of the cell is flattened, and the leukocyte rolls and slides on the adhesive wall. In addition, notice that the front edge of the leukocyte is farther away from the wall and the trailing end which is near the wall is flattened. The flattening increases the surface area over which the adhesion force acts, which is especially critical in the kinetic model, as the distance range over which the force acts is rather small (Cantat 1999 and Khismatullin 2004).

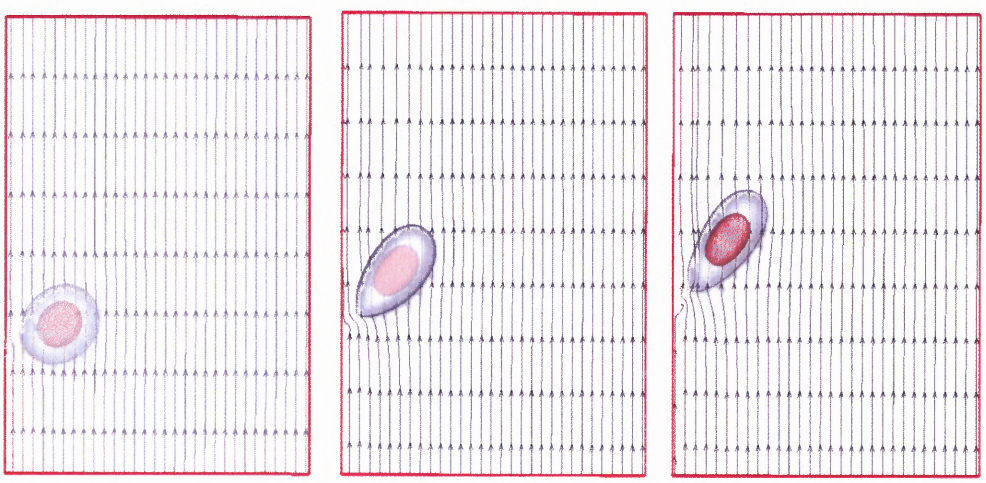

(a) (b) (c)

Figure 7.15 Leukocyte deformation in the case of the compound-drop model and the adhesion force given by the kinetic model. The parameters are selected so that the adhesion force is 100 times larger than for the case shown in Figure 7.14 at (a) t=0.6, (b) t=3 and (c) t=6. The parameters are the same as in Figure 7.14, except Adh=5000.0.

Next consider the influence of the Reynolds number on the time at which the adhesion force becomes zero, i.e., all bonds are broken, and the leukocyte begins to move away. The Reynolds number is varied by increasing the incoming velocity in the channel. From Section 5.3 one can know that as the incoming velocity is increased, the capillary number also increases and the adhesion parameter decreases. Figure 7.16 shows that the leukocyte deformation at higher Reynolds numbers is greater and that it takes a smaller time interval to reach the equilibrium shape. During that time, as the leukocyte deforms, its surface near the wall flattens and it moves slightly towards, and not away from, the wall. This happens to a greater extent at the higher Reynolds numbers. After the surface tension force becomes significant compared to the viscous deforming stress, which occurs when the leukocyte shape is closer to the steady shape, in both cases, it moves away from the wall.

It is worth noting that the hydrodynamic torque on a stretched leukocyte (or any long body) in a shear flow causes it to rotate in the counterclockwise direction. In fact, a rigid long body in a simple shear flow rotates so that it becomes aligned with the flow direction. It is easy to see that in this case the torque pulls the trailing end of the leukocyte away from the wall. Thus, the hydrodynamic torque and the lift force acting on the leukocyte both cause the breakup of the adhesion bonds near the leukocyte's trailing end.

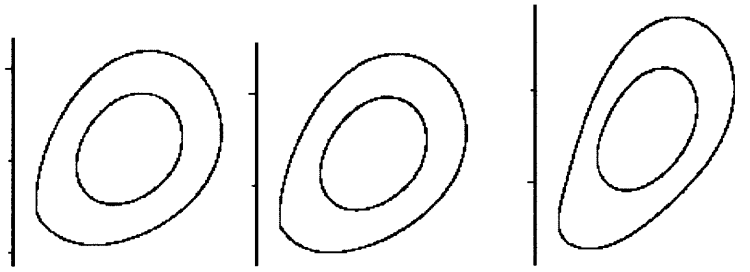

t= 1.2s t=3.0s t=6.3s

(a)

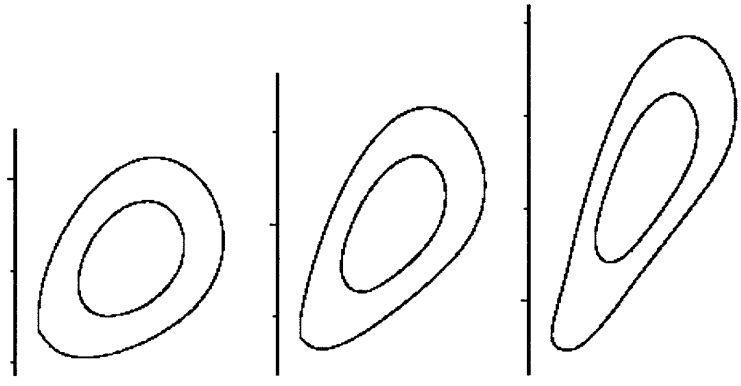

t= 1.2s t=2.4s t=4.2s

(b)

Figure 7.16 Leukocyte sections on the domain mid-plane at different times for two values of the Reynolds number: (a) Re=0.25 and (b) Re=1.

Figure 7.17 shows that the adhesion time decreases with increasing Reynolds number which is expected since the hydrodynamic forces increase with increasing bulk flow velocity. However, the distance traveled by the leukocyte before all bonds are broken, also shown in Figure 7.17, is larger at larger Reynolds numbers, which is due to the fact that the deformation and thus the adhesion force is larger when the Reynolds number is larger. It would be interesting to verify if this is also true for experiments.

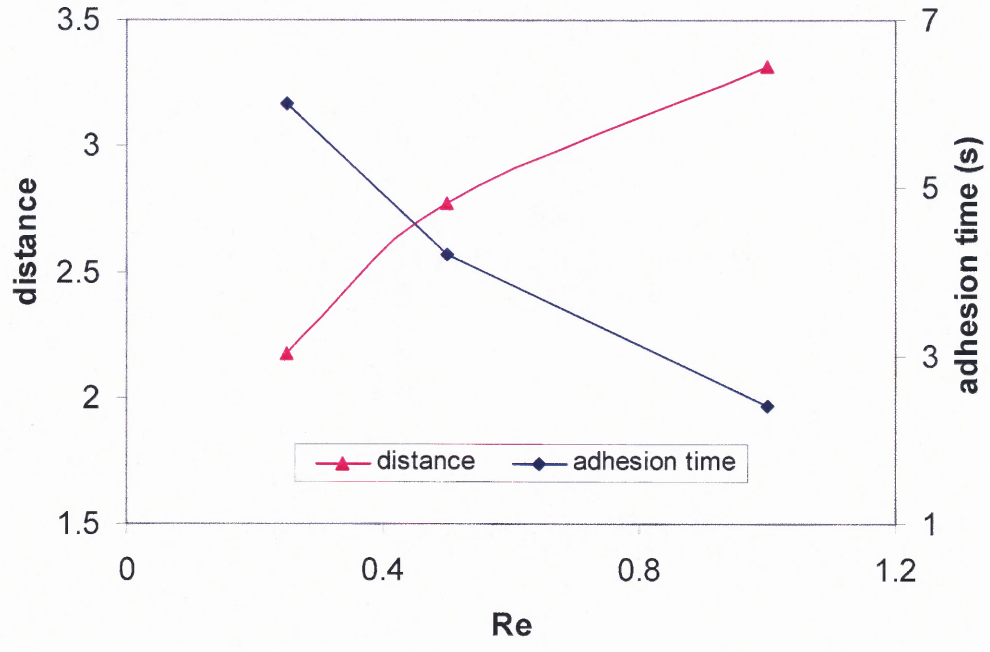

Figure 7.17 The time at which all bonds are broken, and the distance traveled in the flow direction at that time, are shown as functions of Re.

Notice that when the normal parameter values are used in the kinetic model, the adhesive force is much smaller than needed for the capturing of the leukocyte. This is a result of the fact that the distance range over which the force acts is only approximately 30 nm, and thus flattening, which increases the surface area over which the adhesion force acts and the adhesion force, is crucial (Cantat 1999, and Khismatullin 2004). It is therefore important to consider the factors that determine the flattened area. It is known from Section 5.3 that the deformation of a leukocyte increases with increasing capillary number, and that the capillary number depends on the characteristic velocity (assumed here to be the centerline velocity of the pressure driven flow), the plasma viscosity and the cortical tension. In addition, clearly the flattened area over which the adhesion force

acts would be larger if the leukocyte was easier to deform. This suggests that the leukocyte is more likely to remain attached to the wall for higher capillary numbers.

In Figure 7.18, the deformed sections of the leukocyte on the domain mid-plane are shown at different times for two values of the capillary number. The leukocyte deformation at a given time increases with increasing capillary number. For Ca=0.64, the leukocyte is more deformed and the flattened area over which the adhesion force acts is larger and, as a result, the time interval for which it remains attached to the wall is longer than in the case of the smaller Ca shown. However, in all cases considered, the leukocyte drifted away from the wall, indicating that the adhesive force remained smaller than the hydrodynamic force.

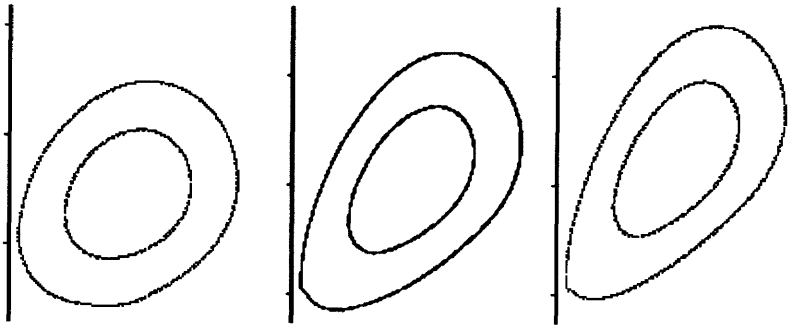

(a) t = 0.6 s t = 1.2s t = 1.5 s

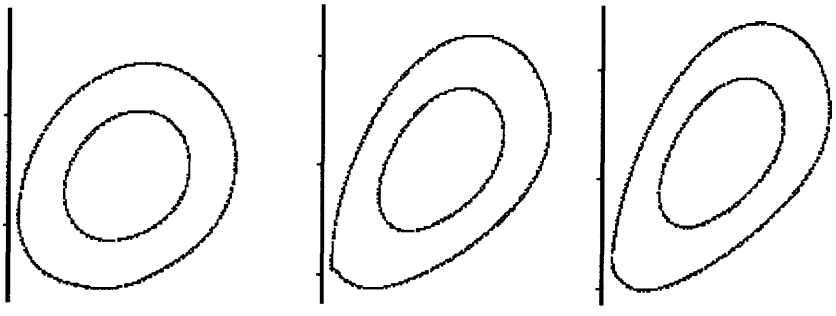

(b) t = 0.6 s t = 1.2 s t = 1.5 s

Figure 7.18 Leukocyte sections on the domain mid-plane at different times for two values of the capillary number. The other parameters are held constant: Re=0.5, De=0.1 and Adh=50.0: (a) Ca=0.64, and (b) Ca=0.32.

In Figure 7.19, the time at which the adhesive force acting on the leukocyte becomes zero, which indicates that the leukocyte is no longer attached to the wall, is plotted as a function of the capillary number. This figure shows that, as concluded above, at larger capillary numbers the leukocyte remains attached to the wall for a longer time. The deformation thus helps in keeping the leukocyte attached to the wall. However, keep in mind that the hydrodynamic lift force also changes when the leukocyte deforms and plays a role in determining the detachment time.

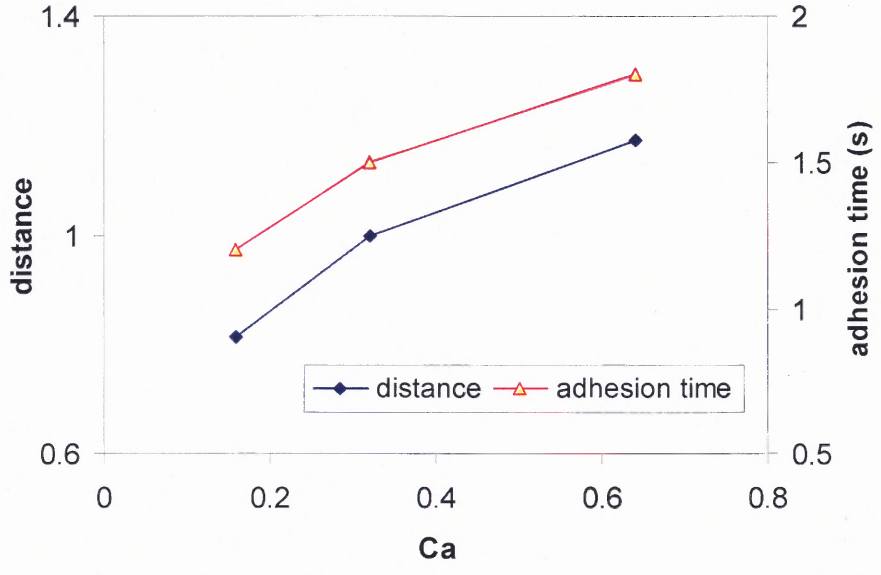

Figure 7.19 The time and distance at which all bonds are broken, and the adhesion force becomes zero, are shown as a function of the capillary number, Ca. The Reynolds number is 0.5, De=0.1 and Adh=50.0.

7.4 Comparison with Experimental Observations

Finally compare these findings with experimental results on the interactions between circulating leukocytes and an endothelial monolayer, it was carried out in a specially designed flow chamber as shown in Figure 7.20 by Chotard-Ghodsnia (2002). They used

a parallel-plate flow chamber to simulate leukocyte and tumor cell extravasation under flow conditions.

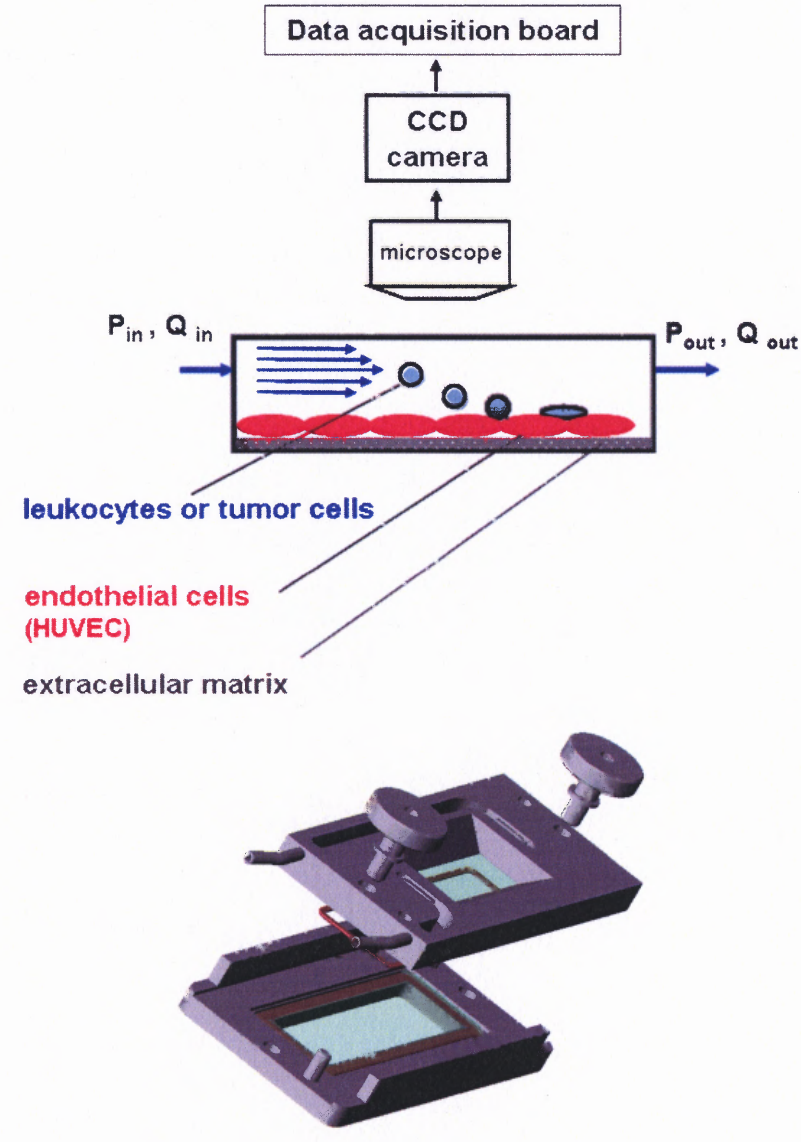

Figure 7.20 Parallel plate chamber system. The motion and deformation of the cells are observed and captured through the top plate by CCD camera. Chotard-Ghodsnia (2002)

A cell monolayer is cultured on the lower plate of the flow chamber to model the endothelial barrier. Leukocytes and circulating tumor cells can be introduced into the flow channel under a well-defined flow field and tumor cell adhesion to endothelial

monolayer can be followed *in situ*. They observed that the cells are attracted to the channel wall as shown in Figure 7.21. Under the flow conditions, some of the cells are strongly adhered to the wall and then they spreading on the wall, but some of them are rolling and may be detached and carried away from the wall by the flow, and may be re-attached on the wall.

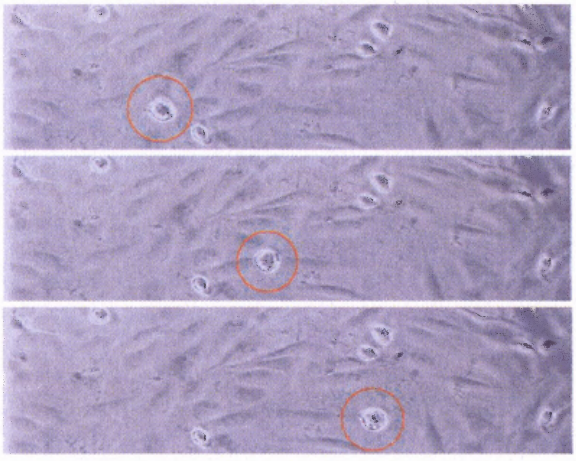

Figure 7.21 Rolling of a leukocyte (inside circles) on the endothelium (view from the top). Other leukocytes are adhering on the substrate wall**.** Chotard-Ghodsnia (2002)

As shown in Figure 7.22(a), the leukocyte, which is already weakly adhering to the endothelium, keeps on rolling and the velocity of rolling exhibits fluctuations. The mean flow velocity is obtained from the applied flow rate and is about 5mm/s, corresponding to physiological conditions. As can be seen from these photographs, the leukocyte is deformed, as it interacts with the endothelial monolayer, and assumes an ellipsoidal shape with its longer axis aligned parallel to the flow direction and the radius of curvature at the leading edge larger than at the trailing edge. This shape resembles the ones described in Figures 7.11 and 7.13. A plot of the instantaneous velocity as a function

of time during rolling of a leukocyte over a significant distance (650 μm) is displayed in Figure 7.22 (b). This shows two kinds of fluctuations:

- small ones attributed to surface roughness, i.e. irregular shapes of endothelial cells with a prominent part in the region where nuclei are located (rolling velocities around an average of 3 μm/s). These fluctuations are similar to those in Figure 7.11 (b) due to the wall unevenness.
- larger ones corresponding to the breaking of a stable filament (reaching velocities up to 15 μm/s)

This latter feature is not considered yet in the model, for it would necessitate the use of local rheological properties enabling the formation and growth of tiny filaments. Similar data have been obtained previously by Jadhav (2005).

Further computations are under way to give access to typical values of the constants used in the model, i.e., k_r and k_f, after combining experimental and theoretical work. More accurate microscopic observations are also needed to determine precisely the distance between the cell and the endothelial wall, as well as the identification of adhesion proteins possibly involved in these mechanisms using fluorescence microscopy.

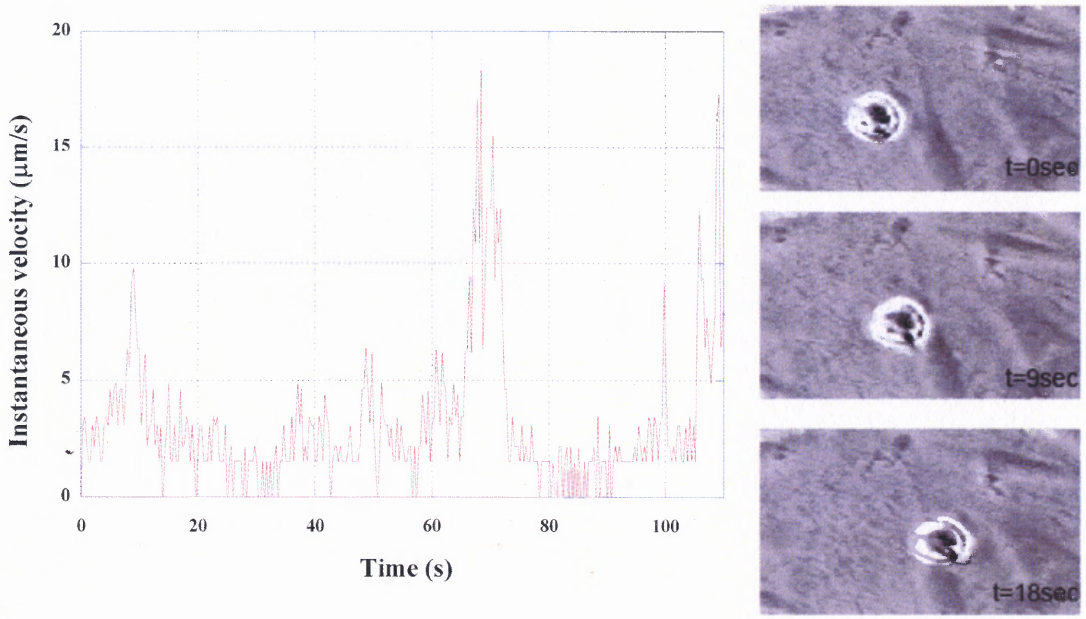

(a) (b)

Figure 7.22 (a) Photographs extracted from a movie of a leukocyte (human neutrophil) rolling along the endothelial monolayer (in grey, phase contrast images). The mean velocity during this sequence is 3.0 μm/s. At the same time, the leukocyte shape changes and elongates. (b) Instantaneous leukocyte velocity with fluctuations.

CHAPTER 8

CONCLUSIONS

Three-dimensional Direct Numerical Simulations of the motion and deformation of a leukocyte in channels with smooth and uneven walls for pressure driven flows are performed. The surface of the leukocyte is tracked using the level set method and in the case of the solid nucleus model the rigid motion enforcement inside the nucleus is performed by using the distributed Lagrange multiplier method. The leukocyte is represented using two different models: the compound-drop model and the drop-rigid-particle model.

The performed simulations show that the leukocyte deformation is larger when it is closer to the wall, where the shear rate is larger. The deformation is smaller for the drop-rigid particle model of the leukocyte. For the parameter values selected, which are typical for such flows, the leukocyte moved away from the wall to a stable location positioned between the center of the channel and the wall. This implies that the adhesion force is necessary for the leukocyte to remain attached to the wall.

The case where the bulk pressure driven flow is not present is also considered. In this case the leukocyte deformed so that its surface near the wall flattened, but it remained attached to the wall since the hydrodynamic force acting on it was zero. In the presence of a pressure driven flow, the leukocyte experienced not only a lift force whose magnitude depends on many parameters including the flow velocity, but also a hydrodynamic torque. Both cause the trailing end of the leukocyte to move away from the wall. Clearly, when the bulk flow velocity is sufficiently small the combined effect of

these hydrodynamic forces is smaller than the adhesive force, and the leukocyte remained attached to the wall. However, when the flow velocity was larger and closer to typical values, the hydrodynamic forces overcame the adhesive force and the leukocyte moved away from the wall. These simulation results showed that for the kinetic model parameter values selected in Section 4.2 and typical flow rates, the leukocyte was found to move away from the wall. In experiments some leukocytes were first rolling on the substrate wall and then carried away by the flow while some of them do get attached to the endothelium monolayer.

It was showed that if the parameters for the kinetic adhesion model were selected as suggested in past studies, the time scale over which the bond density evolved to the equilibrium value was at least an order of magnitude smaller than the flow time scale, and therefore the adhesion force for the fluid dynamics problem could simply be obtained from the steady state version of the kinetic equation.

For the two adhesion models used in this study the trailing end of the leukocyte flattened. The flattening increases the contact surface area over which the adhesion force acts, and thus the adhesion force acting on the leukocyte. The flattening, therefore, plays an important role in increasing the adhesion force so that the latter does not get canceled by the hydrodynamic lift force and torque. The flattening of the leukocyte is particularly crucial for the kinetic model since the distance range over which the corresponding adhesive force acts is approximately 30 nm. The distance range over which the adhesive force given by the potential model acts, on the other hand, is much larger, as it decays as the third power of the distance.

The time at which a leukocyte initially attached to a wall moves away was shown to depend on the capillary and Reynolds numbers. At larger capillary numbers the deformation of the leukocyte was larger. In this case, the leukocyte remained attached for a longer time interval as well as traveled a larger distance in the flow direction since the flattening near the wall was greater which increased the magnitude of adhesive force. On the other hand, when the Reynolds number was increased, the leukocyte moved away from the wall at an earlier time, but traveled a larger distance in the flow direction before detaching from the wall.

The lateral velocity of a leukocyte moving near an uneven wall modeled here as a flat wall covered with a layer of spheres varied with time and it appeared to slip when its trailing end was in the gap between two spheres. In contrast, the lateral velocity near a smooth wall remained approximately constant. The results of the carried out direct simulations agreed qualitatively with the experimental observations and can thus be helpful in predicting the cells deformation during spreading.

CHAPTER 9

FUTURE WORK

9.1 Cell Membrane Elasticity

The current models for leukocyte are limited for very large deformation cases. The elasticity model for cell membrane is requires when the cell undergoes large deformations.

Since the cortical tension is similar as a surface tension only when the cell is under small and moderate deformations. When the large deformation happens, the membrane of the leukocyte will be stretched, and the elasticity of the membrane will limit the deformation.

It is suggested that the cell is surrounded by an infinitely thin elastic membrane, which have a *Mooney-Rivlin* constitutive behavior. The membrane, which is very thin sheet of isotropic elastic solid, obeys a *Mooney* constitutive law, where the strain energy function W per unit area of undeformed membrane material is given by,

$$W = \frac{1}{6}(1-\varphi')[\lambda_1^{\,2} + \lambda_2^{\,2} + (\lambda_1\lambda_2)^{-2} - 3] + \frac{1}{6}\varphi'[\lambda_1^{\,-2} + \lambda_2^{\,-2} + (\lambda_1\lambda_2)^{2} - 3] \tag{9.1}$$

where λ_1, λ_2 are the principal strains using local in-plane curvilinear coordinates. The deformation is conveniently defined in terms of the principal extension ratio λ_1, λ_2 given by,

$$\lambda_1 = \frac{ds}{dS}; \lambda_2 = \frac{r}{R}. \tag{9.2}$$

The parameter φ' measures the nonlinearity of the material, and may vary between 0 and 1. A *neo-Hookean* (linear) material corresponds to $\varphi' = 0$.

9.2 Cytoplasm Modeled as Bingham Fluid (Yield-Stress Fluid)

Experiments results show that cytoplasm in the leukocyte behaves like Bingham fluid. According to Bingham model, the fluid behaves as a rigid solid when the norm of the stress tensor is less than yield stress value. Otherwise, the apparent viscosity of the fluid depends on the shear rate. It can be described mathematically as follows:

$$\tau_{21} = \begin{cases} 0, & |\tau_{21}| < \tau_0 \\ -\mu_0 \dfrac{dv_1}{dx_2} + \tau_0, & |\tau_{21}| \geq \tau_0 \end{cases} \tag{9.3}$$

μ_0 = viscosity parameter

τ_0 = yield stress

Fluids obeying this model exhibit a linear shear-stress, shear-rate behavior after an initial shear-stress threshold has been reached. That is, there is no flow until the shear stress exceeds a critical value called yield stress.

9.3 Interactions between Blood Cells

The modeling carried out in this dissertation is concerned about one singular cell in the flow. The interactions of red blood cells to leukocyte also influences leukocyte's position to the wall and need to be considered in the model.

REFERENCES

1. Burdick, M.M., McCaffery, J.M., Kim, Y.S., Bochner, B.S., Konstantopoulos, K.,. Colon carcinoma cell glycolipids, integrins, and other glycoproteins mediate adhesion to HUVECs under flow. *American Journal of Physiology Cell Physiology* **284**, 977-987, 2003

2. Tözeren, A., Kleinman, H.K., Grant, D.S., Morales, A.M., Byers, S.W., E-selectin-mediated dynamic of breast- and colon cancer-cells with endothelial. *International Journal of Cancer* **60**, 426-431, 1995

3. Haier, J., Nicolson, G. L.. Tumor cell adhesion under hydrodynamic conditions of fluid flow. *APMIS* **109**, 241-262, 2001

4. Evans, E., Skalak, R., Mechanics and Thermodynamics of Biomembranes. *Boca Raton, Boca Raton, FL: CRC*,.101-117, 1980

5. Chotard-Ghodsnia, R., A. Drochon, and Grebe R., A new flow chamber for the study of shear stress and transmural pressure upon cells adhering to a porous biomaterial, *J. Biomech. Eng.* **124**, 258-261, 2002

6. Fung, Y. C., Tong, P., Theory of the sphering of red blood cells**,** *Biophysical journal* **8** (2) , 175-198, 1968

7. Evans, E., Fung, Y. C., Improved measurements of the erythrocyte geometry. *Microvascular research* **4** (4) , 335-347, 1972

8. Evans, E., Yeung, A., Apparent viscosity and cortical tension of blood granulocytes determined by micropipette asporation. *Biophys. J.* **56**, 151-160, 1989

9. Needham, D., Hochmuth R. M., A sensitive measure of surface stress in the resting neutrophil. *Biophysical Journal* **61** (6), 1664-1670, 1992.

10. Hochmuth R.M. Micropipette aspiration of living cells. *Journal of Biomechanics* **33** (1), 15-22, 2000

11. Needham D. and Hochmuth R.M. Rapid flow of passive neutrophils into a 4 μm pipet and measurement of cytoplasmic viscosity. *Journal of Biomechanical Engineering* **112** (3), 269-276, 1990

12. Evans E. and Kukan B. Passive material behavior of granulocytes based on large deformation and recovery after deformation tests. *Blood* **64** (5), 1028-1035, 1984

13. Schmid-Schönbein H., Blood rheology and physiology of microcirculation. *Ricerca in Clinica e in Laboratorio* **11** Suppl 1, 13-33, 1981

14. Drury, J.L. and Dembo, M. Hydrodynamics of micropipette aspiration. *Biophysical Journal* **76**(1), 110-128, 1999.

15. Dong, C., R. Skalak, K, L. P. Sung, G. M. Schmid Schonbein, and S. Chien. Passive deformation analysis of human leukocytes. *J. Biomech. Eng* **110**, 27-36, 1988.

16. Tran-Son-Tay R., Needham, D., Yeung, A., Hochmuth, R.M. Time-dependent recovery of passive neutrophils after large deformation. *Biophysical Journal* **60**(4), 856-866, 1991.

17. Kan H.-C., Udaykumar H.S., Shyy, W., Tran-Son-Tay, R. Hydrodynamics of a compound drop with application to leukocyte modeling. *Physics of Fluids* **10**(4), 760-774, 1998.

18. Shyy, W., Francois, M., Udaykumar, H.S., N'dri, N., Tran-Son-Tay, R. Moving boundaries in micro-scale biofluid dynamics. *Applied Mechanics Reviews* **54** (5), 405-452. 2001.

19. Cox R. G. Deformation of a drop in a general time dependent fluid flow. *Journal of Fluid Mechanics* **37** (pt 3), 601-623, 1969.

20. Acrivos A. Low Reynolds number shear flow past a rotating circular cylinder-1,2 *Journal of Fluid Mechanics* **40** (pt 4), 685-703, 1970.

21. Barthes-Biesel, D., Acrivos A. On computer generated analytic solutions to the equations of fluid mechanics. The case of creeping flows. *Journal of Computational Physics* **12** (3), 403-411, 1973.

22. Choi, H. G., Splitting method for the combined formulation of the fluid-particle problem. *Computer Methods in Applied Mechanics and Engineering* **190** (11-12) , 1367-1378, 2000.

23. Barthes-Biesel. Motion of a spherical microcapsule freely suspended in a linear shear flow. *Journal of Fluid Mechanics* **100** (4), 831-853, 1980.

24. Barthes-Biesel, D., Rallison, J. M. Time dependent deformation of a capsule freely suspended in a linear shear flow. *Journal of Fluid Mechanics* **113**, 251-267, 1981.

25. Barthes-Biesel, D., Sgaier, H. Role of membrane viscosity in the orientation and deformation of a spherical capsule suspended in shear flow. *Journal of Fluid Mechanics* **160**, 119-135 1985.

26. Brunn, Peter O., Gilbert, James, Jiji, Danny, Slow flow of a non-Newtonian fluid past a micro-capsule. *Applied Scientific Research (The Hague)* **40** (3), 253-270 1983.

27. Schmid-Schönbein, H., Wells, R., Goldstone, J., Influence of deformability of human red cells upon blood viscosity. *Circulation research* **25** (2), 131-143, 1969.

28. Goldsmith, H. L., Red cell motions and wall interactions in tube flow. *Federation proceedings* **30** (5), 1578-1590, 1971.

29. Schmid-Schönbein, H., Wells, R., Goldstone, J., Model experiments on erythrocyte Rheology. *Pflugers Archiv European Journal of Physiology* **312** (1) , R39-40, 1969.

30. Fischer, T. M., Stohr-Liesen, M., Schmid-Schonbein, H. The red cell as a fluid droplet: Tank tread-like motion of the human erythrocyte membrane in shear flow. *Science* **202** (4370) , 894-896, 1978.

31. Goldsmith, H. L., Marlow. The flow of model particles and blood cells and its relation to thrombogenesis. *Progress in hemostasis and thrombosis* **1**, 97-127. 1972.

32. Keller, S. R., Skalak, R. Motion of a tank-treading ellipsoidal particle in a shear flow. *Journal of Fluid Mechanics* **120**, 27-47, 1982.

33. Milliken, W. K., Leal, L. G. Deformation and breakup of viscoelastic drops in planar extensional flows. *Journal of Non-Newtonian Fluid Mechanics* **40**(3), 355-379, 1991.

34. Elmendorp, J. J., Maalcke, R. J. Study on polymer blending microrheology: Part 1. *Polymer Engineering and Science* **25**(16), 1041-1047, 1985.

35. Levitt, L., Macosko, C.W., Pearson, S.D., Influence of normal stress difference on polymer drop deformation. *Polymer Engineering and Science* **36** (12), 1647-1655, 1996.

36. K.S.Chang, Olbricht, W. L. Experimental studies of the deformation of a synthetic capsule in extensional flow. *Journal of Fluid Mechanics* **250**, 587-608, 1993.

37. Chang, K.S., Olbricht, W. L., Experimental studies of the deformation and breakup of a synthetic capsule in steady and unsteady simple shear flow. *Journal of Fluid Mechanics* **250**, 609-633, 1993.

38. Bently, B. J., Leal, L. G. Experimental Investigation of drop deformation and breakup in steady, two dimensional linear. *Journal of Fluid Mechanics* **167**, 241-283, 1986.

39. Bently, B. J., Leal, L. G. Computer controlled four-roll mill for investigations of particle and drop dynamics in two dimensional linear shear flows. *Journal of Fluid Mechanics* **167**, 219-240, 1986.

40. Sutera, S.P., Gardner, R.A., Boylan, C.W. Age-related changes in deformability of human erythrocyte. *Blood* **65**(2), 275-282, 1985.

41. Mazeron, P., Muller, S., El Azouzi, H., On intensity reinforcements in small-angle light scattering patterns of erythrocytes under shear. *European Biophysics Journal* **26**(3), 247-252, 1997.

42. Rao, P. R. Effect of electrostatic force on erythrocyte deformation in narrow capillaries. *Advances in Experimental Medicine and Biology* **361**, 555-563, 1994.

43. Li, X. Z., Barthes-Biesel, D., Large deformations and burst of a capsule freely suspended in an elongational flow. *Journal of Fluid Mechanics* **187**, 179-196, 1988.

44. Pozrikidis, C., Finite deformation of liquid capsules enclosed by elastic membranes in simple shear flow. *Journal of Fluid Mechanics* **297**, 123-152, 1995.

45. Zhou, H, Pozrikidis, C., Deformation of liquid capsules with incompressible interfaces in simple shear flow. *Journal of Fluid Mechanics* **283**, 175-200, 1995.

46. Navot. Y., Elastic membranes in viscous shear flow. *Physics of Fluids* **10**(8), 1819-1833, 1998.

47. Pozrikidis, C., Effect of membrane bending stiffness on the deformation of capsules in simple shear flow. *Journal of Fluid Mechanics* **440**, 269-291, 2001.

48. Peskin, C. S., Numerical analysis of blood flow in the heart. *Journal of Computational Physics* **25** (3, Nov.1977), 220-252, 1977.

49. Eggleton, C.D., Popel, A. S., Large deformation of red blood cell ghosts in a simple shear flow. *Physics of Fluids* **10** (8), 1834-1845, 1998.

50. Unverdi, Tryggvason, Collision of a vortex pair with a contaminated free surface. *Physics of Fluids A* **4**(6), 1215-1229, 1992.

51. Haj-Hariri, Thermocapillary motion of deformable drops at finite Reynolds and Marangoni numbers. *Physics of Fluids* **9**(4), 845-855, 1997.

52. Bagge, U., Branemark, P.I., Karlsson, R., Skalak, R., Three-dimensional observations of red blood cell deformation in capillaries. *Blood Cells* **6** (2) , 231-239, 1980.

53. Mohandas, N., Evans, E., Mechanical properties of the red cell membrane in relation to molecular structure and genetic defects. *Annual Review of Biophysics and Biomolecular Structure* **23**, 787-818, 1994.

54. Goldsmith, H.L., Mason, S.G., Further comments on the radial migration of spheres in Poiseuille flow. *Bibliotheca anatomica* **7**, 353-362, 1965.

55. Hiller, W., Lowalewski, T. A., Experimental study of the lateral migration of a droplet in a creeping flow. *Experiments in Fluids* **5** (1), 43-48, 1987.

56. Uijttewaal, W.S.J., Nijhof, E.J., Heethaar, R.M., Lateral migration of blood cells and microspheres in two-dimensional poiseuille flow: A laser-doppler study. *Journal of Biomechanics* **27** (1), 35-42, 1994.

57. Chan. P. C. H., Leal, L. G. Motion of a deformable drop in a second-order fluid. *J Fluid Mech* **92** (pt 1), 131-170, 1979.

58. Zhou, Pozrikidis, C., Motion and deformation of liquid drops, and the rheology of dilute emulsions in simple shear flow. *Computers and Fluids* **23** (2), 251-278, 1994.

59. Couillette, Pozrikidis, C., Motion of an array of drops through a cylindrical tube. *Journal of Fluid Mechanics* **358**, 1-28, 1998.

60. Saeed, M., Tryggvason. A numerical study of the motion of drops in Poiseuille flow. Part 1. Lateral migration of one drop. *Journal of Fluid Mechanics* **411**, 325-350, 2000.

61. Sukumaran S., Seifert U., Influence of shear flow on vesicles near a wall, *Phys. Rev. E.* **64**, 011916, 2001.

62. Dembo M., Torney D. C., Saxman K., Hammer D. The reaction-limited kinetics of membrane-to-surface adhesion and detachment, *Proceedings of the Royal Society of London - B. Biological Sciences* **234**(1274), 55-83, 1988.

63. Bell, G. I., Models for the specific adhesion of cells to cells. A theoretical framework for adhesion mediated by reversible bonds between cell surface molecules. *Science* **200** (4342), 618-627, 1978.

64. Lawrence, M. B., Springer, T. A. Leukocytes roll on a selectin at physiologic flow rates: Distinction from and prerequisite for adhesion through integrins. *Cell* **65** (5), 859-873, 1991.

65. Bell, G. I., Dembo, M., Bongrand, P. Cell adhesion. Competition between nonspecific repulsion and specific bonding. *Biophysical Journal* **45**(6), 1051-1064, 1984.

66. Hammer, D. A., Lauffengurfer, D. A. A dynamical model for receptor-mediated cell adhesion to surfaces. *Biophysical journal* **52** (3), 475-487, 1987.

67. Jin-Yu Shao, Hie Ping Ting-Beall, and Robert M. Hochmuth, Static and dynamic lengths of neutrophil microvilli, *Proc. Natl. Acad. Sci. USA* **95**, pp. 6797–6802, 1998.

68. Evans, E., Parsegian, V. A., Energetics of membrane deformation and adhesion in cell and vesicle aggregation. *Annals of the New York Academy of Sciences* **416**, 13-33 1983.

69. Zhang X., Chen A., De Leon D. Li H., Moy V.T., Goligorski M.S., Atomic force miscroscopy of leukocyte-endothelial interaction, *Am. J. Physiol. Heart Circ. Physiol.* **286**, 359-367, 2004.

70. Thoumine O, Ott A, Time scale dependent viscoelastic and contractile regimes in fibroplasts probed by microplate manipulation, *J. Cell Sci.,* **110**, 2109-2116, 1997.

71. Canetta E., Leyrat A., Verdier C., Duperray A., Measuring cell viscoelastic properties using a force spectrometer: influence of the protein-cytoplasm interactions, *Biorheology* **42**(5), 321-333, 2005.

72. Tsai, M. A., Frank, R.S. and Waugh, R.E. Passive mechanical behavior of human neutrophils: Power-law fluid, *Biophys J.* **65**, 2078-2088, 1993.

73. Lomakina, E. B. Spillmann, C. M. King, M. R. and Waugh, R. E. Rheological Analysis and Measurement of Neutrophil Indentation, *Biophysical Journal*, **87**, 4246–4258, 2004.

74. C. M. Spillmann, E. Lomakina, and R. E. Waugh, Neutrophil Adhesive Contact Dependence on Impingement Force, *Biophysical Journal* **87**, 4237–4245, 2004.

75. Marc Herant, Volkmar Heinrich and Micah Dembo, Mechanics of neutrophil phagocytosis: behavior of the cortical tension. *Journal of Cell Science* **118**(9), 1789-1797, 2005.

76. N'Dri N. A., Shyy W., Tran-Son Tay R., Computational modeling of cell adhesion and movement using a continuum-kinetics approach. *Biophysical Journal* **85**, 2273-2286, 2003.

77. Khismatullin D.B., Truskey G. A. Three-dimensional numerical simulation of a receptor-mediated leukocyte adhesion to surface: Effects of cell deformability and viscoelasticity. *Physics of Fluids* **17**(3), 53-73, 2005.

78. Segré G., Silberberg A., Behavior of macroscopic rigid spheres in Poiseuille flow. Part 2. Experimental results and interpretation, *J. Fluid Mech.* **14**, 136-157, 1962.

79. Lauffenburger D. A., Linderman J. J., Receptors: Models for binding, trafficking, and signaling. *Oxford University Press*, New York. 1993.

80. Bongrand, P. and Bell, G.I. Cell Surface Dynamics: Concepts and Models, Perelson, A. S., DeLisi, C., and Wiegel, F., eds., *Marcel Dekker, Inc. New York*, 459-493, 1984.

81. Hammer, D.A., Apte, S.M., Simulation of cell rolling and adhesion on surfaces in shear flow: General results and analysis of selectin-mediated neutrophil adhesion, *Biophysical Journal* **63**(1), 35-57, 1992.

82. Khismatullin, D.B., Truskey, G.A., A 3D numerical study of the effect of channel height on leukocyte deformation and adhesion in parallel-plate flow chambers, *Microvascular Research* **68**(3), 188-202, 2004.

83. Sussman, M., Semereka, P. & Osher, S., "A level set approach for computing solutions to incompressible two-phase flow," *J. Comput. Phys.* **114**, 146, 1994.

84. Pillapakkam S.B., Singh P., A Level-Set Method for Computing Solutions to Viscoelastic Two-Phase Flow, *Journal of Computational Physics* **174**, 552-578, 2001.

85. Singh P. and Leal L.G., Finite element simulation of the start-up problem for a viscoelastic problem in an eccentric cylinder geometry using third-order upwind scheme, *Theoretical and Computational Fluid Dynamics* **5**, 107-137, 1993.

86. Glowinski, R., Pan, T.W., Hesla, T.I and Joseph, D.D. A distributed Lagrange multiplier/fictitious domain method for particulate flows. *Int. J. of Multiphase Flows.* **25**, 201-233, 1998.

87. Singh P., Joseph D.D., Hesla T.I., Glowinski R.,Pan T.W., Direct numerical simulation of viscoelastic particulate flows, *J. of Non Newtonian Fluid Mechanics* **91**, 165-188, 2000.

88. Singh P. and Joseph D.D., Fluid dynamics of Floating particles, *J. of Fluid Mech.*, **530**, 31-80, 2005.

89. Cantat I., and Misbah C., Dynamics and similarity laws of adhering vesicles in haptotaxis, *Phys. Rev. Lett.* **83**, 235-238, 1999.

90. Jadhav S., Eggleton C.D., Konstantopoulos K., A 3-D computational model predicts that cell deformation affects selectin-mediated leukocyte rolling, *Biophys. J.*, **88**, 96-104, 2005.